Modeling solar radiation on a human body indoors by a novel mathematical model

Yingdong He[1, 2], Edward Arens[2], Nianping Li[1, *], Zhe Wang[3], Hui Zhang[2], Yongga A[1], Chenzhang Yuan[1]

[1] *College of Civil Engineering, Hunan University, Changsha, Hunan 410082, China*
[2] *Center for the Built Environment, University of California, Berkeley, Berkeley, CA 94720, USA*
[3] *Energy Technology Area, Lawrence Berkeley National Lab, 1 Cyclotron Road, Berkeley, CA 94720 USA*
*: Corresponding author. E-mail address: linianping@126.com

Abstract: Solar radiation affects occupant comfort and building energy consumption in ways that have received relatively little attention in environmental design and energy simulation. Direct, diffuse, and reflected irradiation on the body have warming effects that can be equated to increases in the mean radiant temperature (MRT) of the occupant's surroundings. A simplified occupant-centered model (SolarCal Model, i.e., SC Model) has recently been adopted in ASHRAE Standard 55, followed by a comprehensive simulation procedure combining detailed room- and manikin geometries using the Daylight Coefficient Model (DC Model). This paper presents an intermediate-level mathematical model (the HNU Solar Model) capable of rapid annual calculations of the MRT increases. Both the room and occupant geometries are simplified but consistent with those of the SC Model. Novel strategies of the calculation include a sky-annulus fraction, virtual body shadow, and equivalent window. Modeled results are compared with those simulated by the DC Model using *Radiance* software, which is assumed to be accurate. The differences in the Delta MRT by diffuse, direct, and reflected solar radiation are usually less than 1, 2, and 0.5°C between the DC and HNU Solar Models, respectively. For a given occupant position indoors, the HNU Solar Model only needs five seconds to obtain the annual Delta MRT, while the DC Model needs about seven minutes. The HNU Solar Model provides a simple and practical way to evaluate indoor environments at the room scale, to design fenestration, and to predict set-point changes in annual energy simulation of HVAC systems.

Keywords: solar energy; solar radiation; SolarCal Model; Daylight Coefficient Model; HNU Solar Model

Nomenclature

A	total mesh area of the manikin (m^2)	h_1	body height (m)
A_i	mesh area of the i_{th} mesh (m^2)	h_r	radiation heat transfer coefficient ($W/m^2 \cdot K$)
alt	sun altitude (degree)	h_{refl}	equivalent window height (m)
azi	sun azimuth (degree)	I_{diff}	horizontal diffuse radiation outdoors (W/m^2)
azi_{body}	front-body azimuth (degree)	$I_{diff\ actual}$	actual outdoor diffuse radiation for indoor body (W/m^2)
d	window-body distance (m)	$I_{diff\ feet}$	actual outdoor diffuse radiation for indoor feet (W/m^2)
d_0	horizontal deviation of the human body from the window center line (m)	I_{dir}	direct normal radiation outdoors (W/m^2)
d_1	vertical deviation of the human body from the window center line (m)	I_{TH}	total horizontal solar radiation outdoors (W/m^2)
d_{front}	distance between the window-toward body side	MRT	mean radiant temperature (°C)

https://doi.org/10.1016/j.buildenv.2020.107421
https://escholarship.org/uc/item/78f0b543

	and the window (m)		
d_e	equivalent distance between the human body and the equivalent window (m)	n	value related to the window direction
d_{e1}, d_{e2}	deviations of the human body to the center line of the equivalent window (m)	R_{floor}	floor reflectance
d_{feet}	vertical distance between the window center line and the feet (m)	$SHARP$	solar horizontal angle relative to the front of the person (degree)
E_{diff}	solar radiant flux by diffuse radiation (W/m^2)	T_{sol}	window transmittance
E_{dir}	solar radiant flux by direct solar radiation (W/m^2)	w	window width (m)
E_{refl}	solar radiant flux by reflected radiation (W/m^2)	ΔMRT	Delta MRT by solar radiation (°C)
$E_{refl\ diff}$	reflected diffuse radiant flux (W/m^2)	α_{LW}	long-wave absorptivity
$E_{refl\ dir}$	reflected direct radiant flux (W/m^2)	α_{SW}	short-wave absorptivity
$E_{solar,\ i}$	solar radiant flux on the i_{th} mesh (W/m^2)	β	angle between the human body and the window center (degree)
ERF_{solar}	effective radiant field by solar radiation (W/m^2)	γ	angle between the window center line and the sun azimuth (degree)
f_{bes}	body fraction exposed to solar beam radiation	θ_h	horizontal angle of sky view factor (degree)
f_{eff}	body surface fraction exposed to radiation from the environment	$\theta_{h\ eq}$	equivalent horizontal angle (degree)
f_p	projected area factor	θ_v	vertical angle of sky view factor (degree)
f_{svv}	sky view factor	$\theta_{v\ eq}$	equivalent vertical angle (degree)
$f_{svv\ eq}$	equivalent sky view factor	$\theta_{v\ feet}$	vertical angle of sky view factor of the body feet (degree)
$f_{svv\ feet}$	sky view factor of the body feet	$\theta_{v\ sill}$	vertical angle formed by the window sill and the human body center (degree)
h	window height (m)	$\theta_{v\ sill\ feet}$	angle formed by the feet and the window sill (degree)
h_0	window sill height (m)		

1 Introduction

Solar radiation plays an essential role in building environments and energy use. In recent years, numerous studies have been conducted on the use of solar radiation in buildings for electricity generation [1-5], hot water supply [6-8], building ventilation [5], space heating [9, 10], heat recovery [11], and even air purification [12, 13]. Studies also investigated how solar radiation affects floor cooling systems [14, 15]. Worthy of more attention is the effect of solar radiation on human comfort in indoor spaces [16-20]. After entering indoor spaces, solar radiation may heat indoor space and occupants. Such a feature requires set-point corrections to building heating, ventilation, and air conditioning (HVAC) systems [21], which ultimately affects building energy. Therefore, understanding indoor solar radiation is vital for both building environment evaluations and energy use.

Building energy simulations typically address the heat balance of a room under solar gain, converting the transmitted solar radiation into increased air temperatures for calculating air conditioning (AC) load, without considering the effect of the solar radiation landing directly on the room occupants. For example, Fernandes et al. [22] investigated the effects of angular-selective shading systems on HVAC and artificial lighting energy using *EnergyPlus* and *Radiance*. The angular systems were shown to reduce building energy substantially. However, the transmitted radiation was only counted as AC load, and the distribution of solar radiation indoors was only used in the form of

daylight for configuring the lighting control schedule.

An improved step might also consider the increase in the room mean radiant temperatures (MRT) (or radiant asymmetry) from the inside surfaces of walls and windows heated by solar radiation, which lowers thermostat set-points and increases AC load. Zemeureanu et al. [23] developed a computer model for calculating the MRT based on surface temperatures of windows and walls, and found the results were consistent with the experimental results. Guo et al. [24] investigated the MRT of indoor points through computational fluid dynamics (CFD) simulations based on surface temperatures of windows and walls. They found the spatial difference of the MRT was up to 5°C at the 1.3 m horizontal plane, much larger than that of air temperatures, which was up to 2°C. Kim et al. [25] did CFD simulations on performances of cooled panels with a human body indoors (simplified as a cube) and external windows. The results indicate that the window-through solar radiation was the primary source of AC load. In calculating the heat balance of the human body indoors, the long-wave radiation from warm windows and walls heated by solar radiation were included, but the short-wave radiation on the occupant was not.

Some authors calculated solar radiation at several points indoors and then calculated MRT values. Marino et al. [26] studied the influence of solar radiation on indoor thermal environments and building energy consumption (heating, cooling, and lighting). The calculation of solar radiation indoors was based on several points on a horizontal plane indoors. If direct solar radiation hits the point, the MRT includes the increase by direct solar radiation, which then changes indoor set-points. In a heating situation, they found that solar radiation indoors could save up to 40% annual heating energy. Marino et al. [27] also conducted an experimental test to explore the radiant asymmetry caused by solar radiation, doing the measurements at only one point indoors. The results show that the radiant asymmetry by solar radiation was much stronger than those by interior building surfaces like walls, ceilings, and floors. This finding indicates that solar radiation can be the most important one of the indoor radiant heat exchange factors. Gennusa et al. [28] investigated solar radiation indoors and combined it with long-wave radiation from the indoor surfaces. They developed a simple method to convert solar energy and long-wave radiation into the MRT. They combined it with long-wave radiation from the indoor surfaces for evaluating the radiant heat gain of a human body. Gennusa et al. [29] then developed a more comprehensive method that included calculating the MRT impinging on occupants from solar radiation. This method includes calculating angle factors and projected area factors for the human body. To reduce calculation complexity, the models in [28] and [29] use a point to represent the whole human body when calculating solar heat gain. Tzempelikos et al. [30] adopted the method of Gennusa et al. [28] for studying indoor thermal environments near glazed facades. They found that the MRT with solar radiation could be up to 10°C higher than that without solar radiation, resulting in 40% more energy for compensating the overheating of solar radiation than when

sun shades blocked the solar radiation. Similarly, Hwang and Shu [31] also used the method of Gennusa et al. [28] for correcting indoor set-points with considering the transmitted solar radiation, to explore the comfort and energy-saving potential of the glass façade through simulations. They found that the cooling energy might be 50% higher with the increased MRT caused by strong solar radiation than by weak solar radiation. Zhang et al. [32] did a field study in three buildings with a large glass façade. They measured solar radiation at several points indoors, and converted it into the indoor MRT increases. The obtained results indicate that the indoor solar radiation (usually lower than 100 W/m^2) led to an equivalent 1-3°C increase in indoor operative temperatures (2-6 °C increase in the MRT). Zhai [19] reviewed several typical models of the human body heat balance exposed to solar radiation, with indoor parameters as inputs. They also proposed one new model which needs less and more accessible indoor parameters like air temperatures.

Measuring or calculating solar radiation of points indoors provides a simple way to correct indoor set-points. However, it does not precisely represent the solar radiation falling on a human body because the human body is complicated and cannot be simplified as a point. A relatively small projected area is exposed to transmitted direct beam irradiation, while larger body areas are exposed to diffuse-sky and reflected irradiation, via view factors to the areas providing those sources. More importantly, in the design-stage, outdoor climatic parameters, rather than indoor environmental parameters, are more available for environment evaluations and energy simulations. Arens et al. [33] proposed the SolarCal Model (SC Model) to calculate the solar heat gain on the indoor human body. This method includes calculations of direct, diffuse, and reflected solar radiation on the body, converted to an increase in the MRT on the occupant. It has been incorporated by the online CBE Comfort Tool [34] and the ASHRAE Standard 55-2017 [35]. The SC Model is a simplified model used for design purposes requiring minimal inputs about the built surroundings and outdoor radiation conditions. It applies only to clear-sky conditions and assumes a fixed proportion (1:0.2) between direct beam irradiation and diffuse irradiation on the horizontal from an isotropic sky vault. To extend the SC Model to permit detailed annual solar radiation analysis, Zani et al. [36] created the 'Daylight Coefficient Model' (DC Model) capable of simulating hourly solar irradiation on a detailed mesh manikin. The DC Model is based on the Daylight Coefficient method (DC method) in the commercial software *Radiance*, originally developed for predicting daylight or solar radiation distribution on indoor surfaces [37]. In the DC Model, a room model and a detailed mesh manikin consisting of hundreds of surface polygons are established, and *Radiance* is used to simulate total solar radiation falling on the manikin with high precision. Annual simulations of indoor comfort are done using outdoor weather files. The time for an annual room-scale simulation is long (each simulation for one point indoors needs several minutes). The input details (including the manikin) are considerable and may be hard for users to specify early in the design process.

There is a need for a quicker method of computing annual solar radiation falling on a human body indoors using simple inputs. The method would be used both for evaluating window and shading designs and for modeling set-point changes as part of building simulations. In this study, we propose the *HNU Solar Model* to predict the increase in the indoor MRT from solar fluxes absorbed by the occupant. It is intended to have a precision close to that of the DC Model [36], while requiring limited inputs similar to those in the SC Model [33]. Novel strategies of the calculation include a sky-annulus fraction, virtual body shadow, and equivalent windows for diffuse, direct, and reflected solar radiation, respectively, to represent the effects of dynamic factors like sun positions and solar intensities. To evaluate the HNU Solar Model, we compare modeled results with those of the DC Model and a three-day experimental validation in a glazed rooftop chamber. We then compare the features of the DC, SC, and HNU Solar Models, and discuss the applications of the HNU Solar Model.

2. Methodology

2.1 Workflow

The workflow is divided into two branches: one is the experiment work, and the other is the model work (see Fig. 1). The experiment work mainly includes the measurement of indoor and outdoor solar radiation in a chamber, aiming to validate the DC Model by comparing the measured and the simulated solar radiation of several points indoors. The experiment work also provides the chamber geometry and envelope features for the model work. The model work uses *Radiance* to achieve the validation of the DC method. We used *Rhinoceros* and *Grasshopper* to build the room model (based on the chamber geometry and building envelope features in the experiment work) and the manikin model (using the same manikin model as in Zani et al. [36]). After validating the DC method by comparing the measured and the simulated indoor solar radiation at several points, the manikin was added in to establish the entire DC Model. Then the solar radiation on the manikin was simulated. The solar radiation absorbed by the manikin was finally converted into the Delta MRT.

Meanwhile, we also used our new HNU Solar Model to calculate the solar radiation absorbed by the human body. The HNU Solar Model is a mathematical model, and it is coded in Python and inserted in *Grasshopper*. The detailed information of the DC, SC, and HNU Solar Models is listed in section 2.3.

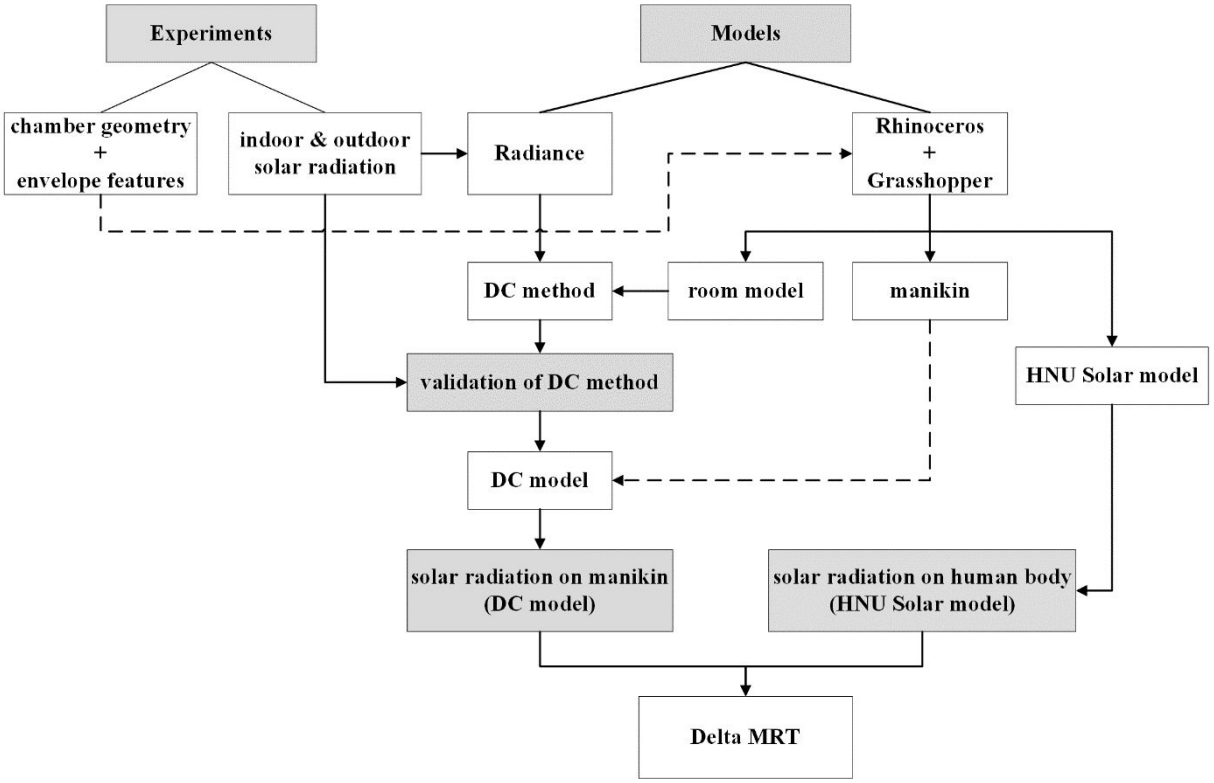

Fig. 1. The workflow of this study.

2.2 Experiments

2.2.1 Facility

The experimental work of measuring indoor and outdoor solar radiation was conducted in a chamber located on the roof of a lab building at Hunan University (Fig. 2(a)). The measurement period was from September 30th to October 1st, with sunny weather through these three days. During the test period, the total horizontal solar radiation outdoors varied from 0-800 W/m^2 (see Fig. 10), covering the main scope of the solar radiation intensity that a region might experience throughout the year. Therefore, outdoor solar radiation during the test period can represent practical weather conditions for model configurations and validations.

The interior size of the chamber was 4.5 m × 3.4 m × 2.8 m (length × width × height). The wall of the chamber was flexible and made of steel sandwich panels with a 100-mm-thick polyurethane layer inside. The chamber roof had a two-level construction. The lower level, which included the ceiling of the chamber, was made by steel sandwich panels, and suspended aluminum ceiling panels sheltered its interior surface. The higher level was inclined and made of water-proof steel. An air gap between the lower and the higher levels provided ventilation to reduce heat transfer from solar radiation. Carpets with dark colors covered the floor. Besides, the chamber had large flexible windows on the east, south, and west walls. In this study, the south, north, and east windows were covered with opaque panels made of plastic extruded boards. The interior colors of the walls and ceiling were white. The west window was unsheltered and

consisted of single-pane glass (transmittance 0.8) with a dimension of 4.3 m × 2.2 m (width × height). With the west window, the indoor space of the chamber mainly had two conditions: (1) diffuse solar radiation only (in the morning), and (2) both diffuse and direct solar radiation with various sun altitudes (in the afternoon). These two conditions cover many of the radiation conditions encountered indoors, giving the validation tests some universality.

As shown in Fig. 2(b), two positions (A and B) for measuring indoor solar radiation were set up in the chamber, with 1 and 2.2 m distances from the west window, respectively. Each position had two TBQ-2 solar radiation sensors (one vertical and the other horizontal), which measured the total solar radiation every five minutes with the accuracy of ±1 W. The vertical sensors were at the 0.5 m height from the floor while the horizontal was at the 0.1 m height. The horizontal distance between the vertical and the horizontal sensors at each position was 0.5 m. Outdoor solar radiation was measured by the TBS-YG1 solar radiation measuring system with the accuracy of ±1 W (see Fig. 2(c)). The system was installed on another four-story building roof which was about 20 m to the south of the chamber and was about 10 m higher than the roof where the chamber was located. The system's location was flat and open, higher than the ambient buildings and trees, which ensured that the sunshine falling on the system was not blocked. During the tests, the outdoor solar radiation measuring system measured the horizontal diffuse, direct normal, and horizontal total solar radiation every five minutes.

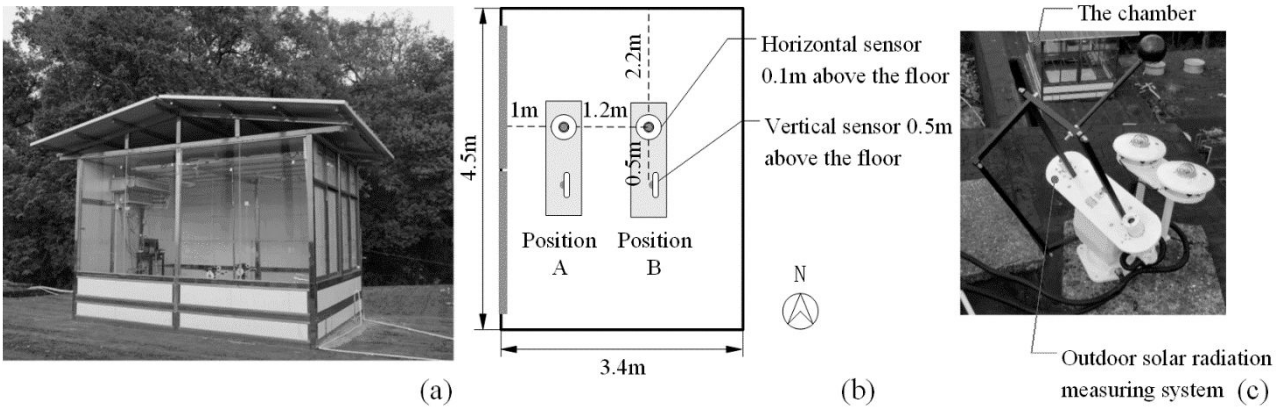

Fig. 2. Test chamber: (a) the onsite scene of the west side, (b) the indoor layout, and (c) the outdoor solar radiation measuring system.

2.3 Models

2.3.1 DC method and DC Model

The DC method in *Radiance* was originally designed to simulate lighting and daylighting of indoor and outdoor environments. The DC method uses three-dimension vectors to simulate solar radiation distribution. Through analyzing the vectors falling on an object, the detailed solar flux or the illumination can be obtained. The DC method was used by Zani et al. [36] to simulate solar radiation on the human body surface by inserting a manikin model of hundreds of small

surfaces within a room model. Zani's paper [36] presents details about how the DC method works in *Radiance* and how to build a manikin to complete the whole DC Model. Here, we focus on how the DC method and the DC Model were used in this study.

First, the DC method was used to simulate the solar radiation at four indoor points (see Fig. 2(b)) to ensure that the DC method was properly set up. A rofom model was established using *Rhinoceros* and *Grasshopper* based on the chamber geometry (see Fig. 3). The reflectance ratios of indoor ceiling (aluminum ceiling panels), floor (with dark color carpets), and the wall (steel sandwich panels) were set as 0.3, 0.1, and 0.2, respectively. The transmittance of the window was 0.8. Four small meshes (two vertical and two horizontal, 4 cm × 4 cm each) were set up in the room model according to the positions of four measurement points shown in Fig. 2(b). Then, in *Radiance*, the Gendaymtx tool was used to generate a simulated sky using the measured outdoor direct and diffuse solar radiation. And the Rfluxmtx, Dctimestep, and Rmtxop modules were used to calculate the daylight matrixes, multiply matrixes, and convert daylight to radiation, respectively. Afterward, the simulated solar radiation of the four points was obtained by running *Radiance*, and then compared with the measured data to validate the reliability of the DC method.

Based on the work above, Zani's 1.32 m-high seated manikin of 363 mesh polygons was built and set up inside the room model (see Fig. 3) to complete the DC Model. For the manikin, each mesh centroid had a sensor point oriented with a normal outgoing to the centroid surface. Thus *Radiance* only calculates the solar radiation falling on the exterior side of each mesh. The skyMatrix, RADPaGridBased, and DCoeffGBRecipe modules in *Grasshopper* were used to initialize and run the *Radiance* simulation.

The SC Model (see section 2.3.2) and HNU Solar Model (see section 2.3.3) assume that the reflected solar radiation reaching the manikin is mainly from the floor. Therefore, when simulating the solar radiation on the manikin, the reflectance ratios of the indoor ceiling, floor, and wall were set as 0, 0.2, and 0, respectively. Therefore, the DC Model only has reflected radiation from the floor. The trunk center of the manikin had four different distances to the window: 0.5, 1.0, 1.5, and 2.0 m (we did not set horizontal deviation from the window center line).

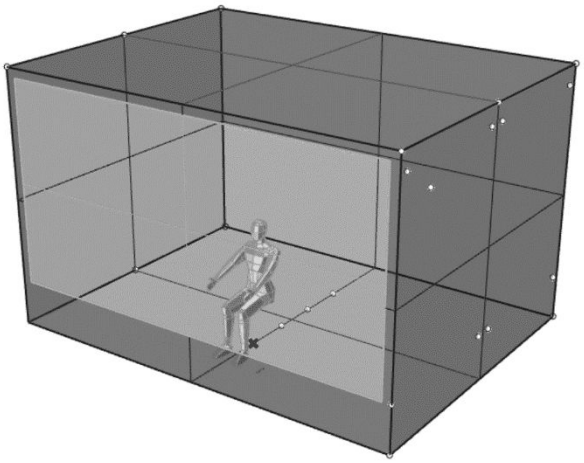

Fig. 3. The room model and manikin of the DC Model.

After the solar radiation on each mesh of the manikin was obtained, the effective radiant field was calculated and converted into Delta MRT [36]:

$$ERF_{solar} = \frac{\alpha_{SW}}{\alpha_{LW}} \sum_{i=1}^{363} \frac{E_{solar,i} A_i}{A} \quad (1)$$

$$\Delta MRT = \frac{ERF_{solar}}{f_{eff} h_r} \quad (2)$$

where ERF_{solar} is the effective radiant field by solar radiation (W/m^2). Effective radiant field is a measure of the net radiant energy flux to or from the human body [33]. $E_{solar,\,i}$ is the short-wave solar radiant flux on the i_{th} mesh (W/m^2), A_i is the mesh area of the i_{th} mesh (m^2), A is the total mesh area of the manikin (m^2), f_{eff} is the body surface fraction exposed to radiation from the environment (=0.696 for a seated person), h_r is the radiation heat transfer coefficient (=6.012 W/m^2·K), α_{SW} is the short-wave absorptivity (=0.67), α_{LW} is the long-wave absorptivity (=0.95), and ΔMRT is the Delta MRT by solar radiation. It should be noted that α_{SW} presents the effects of the human skin color as well as the color and amount of clothing covering the body. The α_{SW} value is set at 0.67 in this study for the white skin and average clothing [33]. The α_{SW} value can also be set at different values if the specific information about the clothing or skin color of the occupants is available.

2.3.2 SC Model

The SC Model was proposed and presented in Arens' paper [33], and then it was somewhat simplified and included in ASHRAE Standard 55-2017 [35]. The SC Model is purely mathematical, and it does not require modeling room geometry. The SC Model includes three types of solar radiation (diffuse, direct, and reflected solar radiation), which may fall on a human body near a window. The calculation of solar radiant flux of three types of solar radiation on an indoor human body is listed as below:

$$E_{diff} = 0.5 f_{eff} f_{svv} T_{sol} I_{diff} \quad (3)$$

$$E_{dir} = f_{eff} f_p f_{bes} T_{sol} I_{dir} \quad (4)$$

https://doi.org/10.1016/j.buildenv.2020.107421
https://escholarship.org/uc/item/78f0b543

$$E_{refl} = 0.5\left[\sin I_{dir} sin\ (alt)\ + I_{diff}\right] \times f_{svv} f_{eff} T_{sol} R_{floor} \qquad (5)$$

where E_{diff}, E_{dir}, and E_{refl} are the solar radiant flux by diffuse, direct, and reflected solar radiation (W/m^2), respectively, and f_p is the projected area factor (ASHRAE Standard 55-2017 Appendix C [35] provides a computer program to calculate it (we adopt the same computer code but written in Python in this study)). f_{bes} is the fraction of the body exposed to the solar beam radiation (in ASHRAE Standard 55 [35], it is equal to the fraction of the distance between the head and toe exposed to direct sun), T_{sol} is the window transmittance (=0.8 in this study), f_{svv} is the sky view factor (the calculation is described in section 2.3.3.1), I_{dir} is the direct normal solar radiation outdoors (W/m^2), *alt* is the solar altitude, I_{diff} is the diffuse solar radiation on a horizontal outdoors (W/m^2), and R_{floor} is the floor reflectance (=0.2 + 0.3. 0.2 is the actual floor reflectance. 0.3 is an approximation for the long-wave radiation emitted upward from absorbed short-wave radiation to the floor). The factors 0.5 reflect the directionality of diffuse (downward) and reflected (upward) radiation on the body.

Then the effective radiant field can be calculated based on the sum of E_{diff}, E_{dir}, and E_{refl}.

$$ERF_{solar}\left[0.5 f_{svv}\left(I_{diff} + I_{TH} R_{floor}\right) + f_p f_{bes} I_{dir}\right] f_{eff} T_{sol}\left(\frac{\alpha_{sw}}{\alpha_{lw}}\right) \qquad (6)$$

where I_{TH} is the total horizontal solar radiation outdoors (W/m^2) (= $\sin I_{dir} sin\ (alt)\ + I_{diff}$).

Subsequently, the Delta MRT by solar radiation is calculated by using Eq. (2).

2.3.3 HNU Solar Model

Our new model is called the HNU Solar Model, for Hunan University where this study was mainly conducted and completed. The HNU Solar Model calculates diffuse, direct, and reflected solar radiation, and finally converts the total solar radiation into Delta MRT. The new model is based on the SC Model, and meanwhile, many revisions are added to allow calculation of certain details of room/window geometry.

2.3.3.1 Diffuse radiation calculation

In the HNU Solar Model, calculations of f_{svv} and I_{diff} in Eq. (3) are elaborated as follows.

Calculation of f_{svv}. Sky view factor (f_{svv}) is the fraction of sky to which a human body is exposed. In the SC Model [33], f_{svv} is roughly estimated by the angle of a human body relative to a window. The angle can be divided into two directions: the horizontal angle (θ_h) and the vertical angle (θ_v). These two angles are estimated by the window height (h), window width (w), and the distance between the window and the body (d). f_{svv} is calculated below [33]:

$$f_{svv} = \frac{\frac{\theta_h}{2} \times \frac{\theta_v}{2}}{90 \times 180} = \frac{tan^{-1}\left(\frac{h}{2d}\right) \times tan^{-1}\left(\frac{w}{2d}\right)}{90 \times 180} \qquad (7)$$

The SC Model does not consider the effects of the window sill height (h_0), body height (h_1) (=1.32 m for a seated person in this study), or the Cartesian position of the body in the room. We use a more detailed approach to calculate the sky view factor, the *sky-annulus fraction method*, which incorporates the window, window sill, and human body positions. As shown in Fig. 4(a), the sky annulus for a given sky view factor is a circle-like area in the sky hemisphere

(the area surrounded by solid and dashed red lines), which corresponds to the sky view factor in the vertical direction (the vertical angle θ_v). θ_v is decided by the window height (h), window sill height (h_0), the distance between the window and the body (d), and the vertical deviation of the human body from the window center line (d_1, $=0.5h + h_0 - 0.5h_1$). Then, we calculate the fraction of the sky annulus (the solid red line in Fig. 4(b)) that the human body sees through the window. The fraction of the sky annulus corresponds to the sky view factor in the horizontal direction (the horizontal angle θ_h). θ_h is decided by the window width (w), the distance between the window and the body (d), and the horizontal deviation of the human body from the window center line (d_0). f_{svv} is the ratio of the fractional annulus area to the whole sky area. Therefore, f_{svv} is calculated as below:

$$f_{svv} = [\sin sin\ (\theta_v + \theta_{v\_sill}) - \sin sin\ \theta_{v\_sill}\ ] \times \frac{\theta_h}{360} \qquad (8)$$

where θ_{v_sill} is the vertical angle formed by the window sill and the human body center (as shown in Fig. 4(b)). When the human body center is higher than the upper boundary of the window sill, θ_{v_sill} is zero; when the human body center is lower than the upper boundary of the window sill, θ_{v_sill} is $\tan^{-1}[(d_1\text{-}0.5h)/d]$. The horizontal angle ($\theta_h$) and the vertical angle (θ_v) are calculated as below:

$$d_1 \le \frac{h}{2}: \quad \sin sin\ (\theta_v + \theta_{v\_sill}) - \sin sin\ \theta_{v\_sill} = sin(tan^{-1}\frac{\frac{h}{2}+d_1}{d}) \qquad (9)$$

$$d_1 > \frac{h}{2}: \quad \sin sin\ (\theta_v + \theta_{v\_sill}) - \sin sin\ \theta_{v\_sill} = sin(tan^{-1}\frac{d_1+\frac{h}{2}}{d}) - sin(tan^{-1}\frac{d_1-\frac{h}{2}}{d}) \qquad (10)$$

$$d_0 \le \frac{w}{2}: \quad \theta_h = tan^{-1}\frac{\frac{w}{2}+d_0}{d} + tan^{-1}\frac{\frac{w}{2}-d_0}{d} \qquad (11)$$

$$d_0 > \frac{w}{2}: \quad \theta_h = tan^{-1}\frac{d_0+\frac{w}{2}}{d} - tan^{-1}\frac{d_0-\frac{w}{2}}{d} \qquad (12)$$

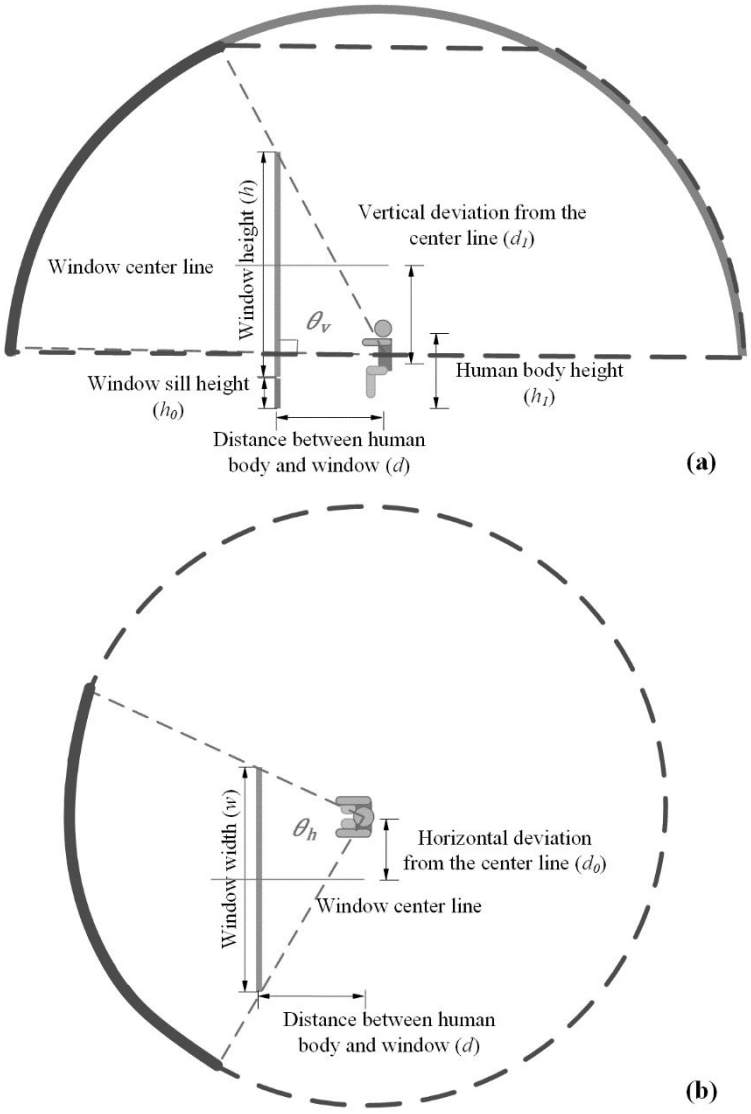

Fig. 4. Diffuse solar radiation parameters: (a) the vertical view and (b) the horizontal view

Calculation of I_{diff}. In the SC Model, the diffuse solar radiant intensity is assumed uniform across the sky. Therefore, the horizontally-measured diffuse solar radiation outdoors is used for calculating solar radiation on the indoor human body. In the HNU Solar Model, we use a non-uniform radiant intensity distribution abstracted from the study of Steven and Unsworth [38]. Fig. 5(a) shows the clear sky divided into two quarter-spheres [38]: the sun quarter-sphere (in orange) exhibits local diffuse radiant intensities that are much greater near the sun position, reaching five or more times the total horizontally-measured value. The radiation intensity at the sun position is linearly correlated with sun altitude (*alt*). The no-sun quarter sphere (in blue) has relatively uniform radiant intensities ranging between 0.5 and 1 times the total horizontally measured value. The HNU Solar Model treats the diffuse intensity at a certain point in the sky as the sum of the base diffuse radiation (same as the average diffuse radiation intensity of the no-sun quarter sphere) and the extra diffuse radiation due to the sun position. Based on reference [38], we propose a simplified method

to calculate the diffuse radiation transmitted through a window onto the human body. As shown in Fig. 5(b), γ is the angle between the window center line (towards indoors) and the sun azimuth (azi), and is calculated as below:

$$\gamma = azi - 90n \qquad (13)$$

where n is a value related to the window direction (=1 (east), 2 (south), 3 (west), 4 (north)). When γ is between -90 and 90 degrees, direct solar radiation enters indoor space. In Fig. 5(b), β is the angle between the human body and the window center, and it can be calculated by using d_0 and d. When the body is on the right side of the window center line, β is positive. When $\beta - \gamma$ is between -90 and +90 degrees, the body sees the sun quarter sphere through the window. Here, the diffuse radiation of a point in the sky is assumed to linearly decrease with the altitude deviation ($alt - 0.5\theta_v$ - θ_{v_sill}) and the azimuth deviation ($\beta - \gamma$) from the sun position. According to the angles in Fig. 5(b), the actual outdoor diffuse radiation for the indoor body (I_{diff_actual}) is:

$$I_{diff\_actual} = 0.8I_{diff} + (4.7 - 0.05\times alt) \times I_{diff} \times \frac{(90-|alt-0.5\theta_v-\theta_{v\_sill}|)\times(90-|\beta-\gamma|)}{90\times 90} \qquad (14)$$

It should be noted here that we assume in Eq. (14) is that a point diffuse radiation intensity can be used to represent the whole window-transmitted diffuse radiation on the body. Thus Eq. (14) may overestimate the diffuse radiation when the window is huge and the occupant is close to it.

When the body is exposed to the no-sun quarter sphere since the diffuse radiation is relatively uniform, the actual diffuse radiation is simplified as below:

$$I_{diff\_actual} = 0.8I_{diff} \qquad (15)$$

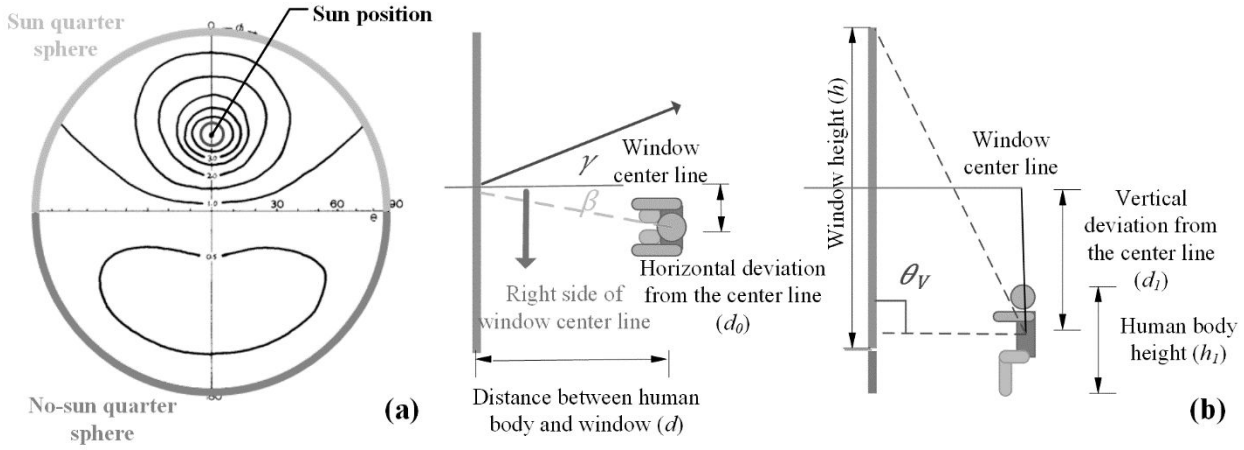

Fig. 5. Diffuse solar radiation calculation: (a) the non-uniform sky (originally from reference [38]), and (b) angles for calculating transmitted diffuse radiation intensity

Based on the revisions above, the calculation of diffuse radiation on a human body indoors is expressed as below:

$$E_{diff} = 0.5f_{eff}f_{svv}T_{sol}I_{diff\_actual} \qquad (16)$$

2.3.3.2 Direct radiation calculation

As for direct radiation, in the SC Model (Eq. (4)), only f_p and f_{bes} need to be calculated. For the HNU Solar Model, we propose the following more detailed ways to calculate the two variables.

Calculation of f_p. f_p is calculated by using the sun altitude (*alt*) and the sun horizontal angle relative to the front of the person (*SHARP*). When using the SC Model, SHARP values are defined by the users. In the HNU Solar Model, *SHARP* can be calculated by the sun azimuth (*azi*) and front-body azimuth (azi_{body}):

$$SHARP = \left| azi - azi_{body} \right| \qquad (17)$$

azi_{body} is similar to the *azi*: when the front-side of the human body towards north, east, south, and east, azi_{body} is 0, 90, 180, and 270 degrees, respectively.

Calculation of f_{bes}. The SC Model is used only when the occupant is impacted by direct beam sunlight. The user approximates the fraction of the body (f_{bes}) exposed to the beam. The HNU Solar Model applies to both sun and no-sun conditions, so before calculating f_{bes}, it is necessary to determine whether direct solar radiation enters the indoor space through the window. When γ, calculated by Eq. (13), is between -90 and 90 degrees, direct solar radiation enters indoor space.

The calculation of f_{bes} is based on projections of the body and the window. In ASHRAE Standard 55-2017, f_{bes} equals the fraction of the distance between the head and toe exposed to direct sun (see Fig. 6(a)). In the HNU Solar Model, the seated body is also simplified as a 1.32 m vertical line, corresponding to the height of the manikin of the DC Model. When direct radiation enters the room, there is a reflected area, which is the window projection on the floor (see Fig. 6(c)). When the human body is exposed to the direct solar radiation, only the body side toward the window is exposed, while the other side is shadowed. The body side toward the window is closer to the window than the middle of the body trunk. Therefore, the distance between the window-facing body side (the average distance of the leg front and the trunk front) and the window (d_{front}) is used to calculate f_{bes} instead of d, which is the distance between the trunk middle and the window (see Fig. 6(b)). We define the distance from the trunk middle of the DC manikin to the window-facing side of the body to be 0.1 m:

$$d_{front} = d - 0.1 \qquad (18)$$

Then, as shown in Fig. 6(c), we define the concept of the virtual body shadow (the solid red line), which is the shadow of the window-toward body side on the floor when there are no surrounding shading sources (assuming that the whole building is removed). The length of the virtual body shadow is decided by the human body height (h_1) and the sun altitude, i.e., $h_1/\tan(alt)$. f_{bes} equals the fraction of the virtual body shadow overlapped with the reflected area (the orange area in Fig. 6(c)). When the body is exposed to the direct radiation ($f_{bes}>0$), there must an overlapped area of the virtual body shadow and the reflected area, and the location of the window-toward body side must be between the two dashed blue lines in Fig. 6(c). This circumstance can be expressed as:

$$d_0 - d_{front} \times \tan tan\ (\gamma) \ < \ \tfrac{w}{2} \qquad (19)$$

https://doi.org/10.1016/j.buildenv.2020.107421
https://escholarship.org/uc/item/78f0b543

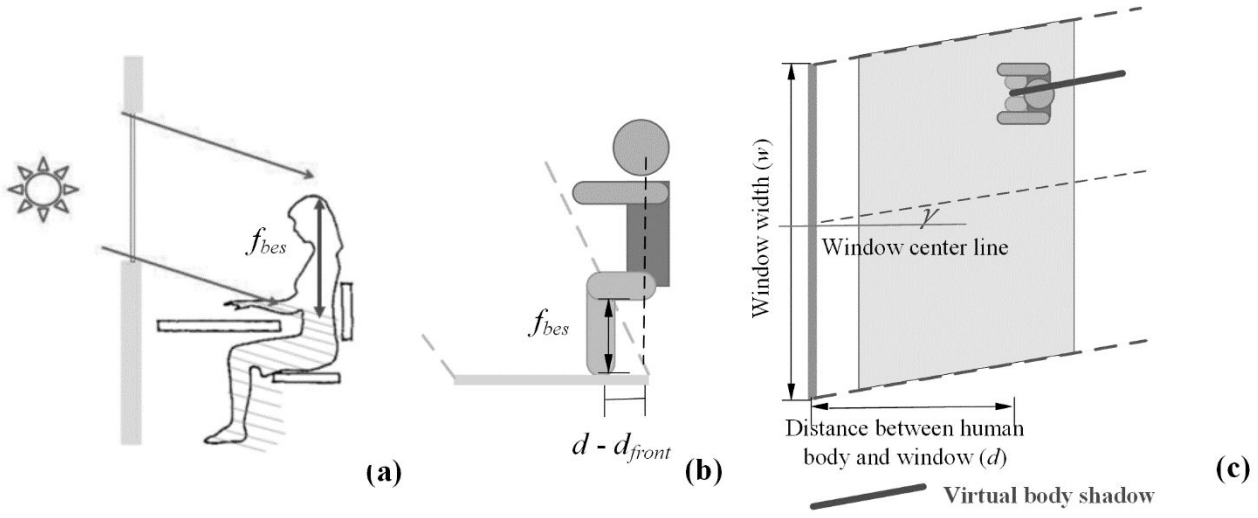

Fig. 6. Direct solar radiation calculation: (a) the f_{bes} defined in ASHRAE Standard 55, (b) the body location correction, and (c) the virtual body shadow

When the location of the window-toward body side is between the two dashed blue lines in Fig. 6(c), there are six different conditions for determining f_{bes} (see Fig. 7).

(1) When the window-toward body side location is in the reflected area:

$$\frac{h_0+h}{tan(alt)} > \frac{d_{front}}{cos(\gamma)} \geq \frac{h_0}{\tan tan\,(alt)} \qquad (20)$$

1) When the virtual body shadow is entirely in the reflected area (Fig. 7(a)):

$$\frac{h_0+h}{tan(alt)} \geq \frac{d_{front}}{\cos cos\,(\gamma)} + \frac{h_1}{\tan tan\,(alt)} : \qquad f_{bes} = 1 \qquad (21)$$

2) When the virtual body shadow is partly within the reflected area (Fig. 7(b)):

$$\frac{h_0+h}{tan(alt)} < \frac{d_{front}}{cos(\gamma)} + \frac{h_1}{tan(alt)} : \qquad f_{bes} = \frac{\frac{h_0+h}{tan(alt)} - \frac{d_{front}}{cos(\gamma)}}{\frac{h_1}{tan(alt)}} \qquad (22)$$

(2) When the window-toward body side location is not in the reflected area but close to the window:

$$\frac{d_{front}}{cos(\gamma)} < \frac{h_0}{tan(alt)} \qquad (23)$$

1) When the top of the virtual body shadow is in the reflected area (Fig. 7(c)):

$$\frac{h_0+h}{tan(alt)} \geq \frac{d_{front}}{\cos cos\,(\gamma)} + \frac{h_1}{\tan tan\,(alt)} > \frac{h_0}{\tan tan\,(alt)} : \qquad f_{bes} = 1 - \frac{\frac{h_0}{\tan tan\,(alt)} - \frac{d_{front}}{\cos cos\,(\gamma)}}{\frac{h_1}{\tan tan\,(alt)}} \qquad (24)$$

2) When the top of the virtual body shadow is beyond the reflected area (Fig. 7(d)):

$$\frac{d_{front}}{\cos cos\,(\gamma)} + \frac{h_1}{\tan tan\,(alt)} > \frac{h_0+h}{tan(alt)} : \qquad f_{bes} = \frac{h}{h_1} \qquad (25)$$

3) When the ***TOP*** of the virtual body shadow does not reach the reflected area (Fig. 7(e)):

$$\frac{h_0}{tan(alt)} \geq \frac{d_{front}}{\cos cos\,(\gamma)} + \frac{h_1}{\tan tan\,(alt)} : \qquad f_{bes} = 0 \qquad (26)$$

(3) When the window-toward body side is not in the reflected area and far away from the window (Fig. 7(f)):

$$\frac{d_{front}}{cos(\gamma)} \geq \frac{h_0+h}{\tan tan\,(alt)} : \qquad f_{bes} = 0 \qquad (27)$$

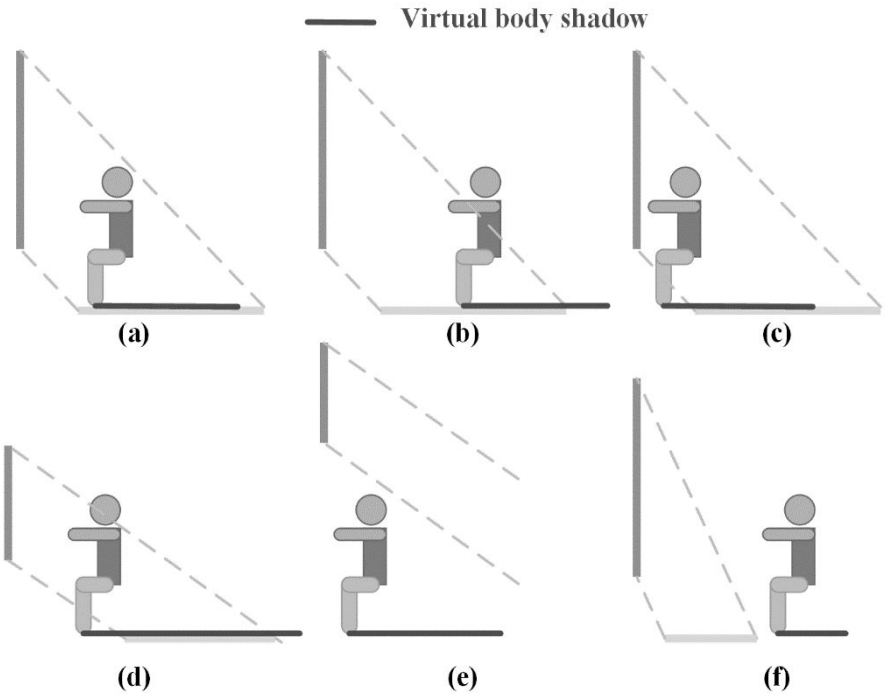

Fig. 7. Direct solar radiation calculation: six relative locations of the human body to the reflected area

2.3.3.3 Reflected radiation calculation

In practice, for low-rise building space, the reflected solar radiation from the outdoor ground is usually blocked by the window sill and surroundings (like trees and other buildings). Therefore, in the HNU Solar Model, the reflected solar radiation is assumed to be from the indoor ground (floor).

The reflected solar radiant flux on the human body can be divided into two parts: one is the reflected direct radiant flux (E_{refl_dir}), and the other is the reflected diffuse radiant flux (E_{refl_diff}). Four assumptions are made in the HNU Solar Model for calculating the reflected solar radiation on the human body:

(1) The reflected radiation is mainly from the indoor floor.

(2) The indoor floor only has a diffuse reflection rather than a mirror reflection.

(3) The reflected diffuse radiation on the human body is mainly from the floor near the occupant's feet.

(4) The body fraction that could receive the reflected radiation is the same as the f_{eff}.

Calculation of $\boldsymbol{E_{refl\_dir}}$. As stated in section 2.3.3.2, when direct solar radiation enters indoor space, there is a reflected area on the floor (see Fig. 8), which is affected by the window size, window direction, and sun position. According to the assumptions above, the reflected area is treated as an equivalent roof window at the head-top height (see Fig. 8, and the red circle is the center of the equivalent window). Since the floor is assumed to have only diffuse reflection, the reflected direct radiation (E_{refl_dir}) from the reflected area can be regarded as the equivalent diffuse radiation from the equivalent roof window with the 1.0 transmittance. Then a similar method as that for calculating

diffuse radiation in section 2.3.3.1 is used for the calculation of the reflected direct radiation. The equivalent diffuse radiation (I_{diff_eq}) equals to the horizontal direct radiation times the floor reflectance ratio:

$$I_{diff\_eq} = T_{sol} R_{floor} I_{dir} \sin sin\ (alt) \qquad (28)$$

And the reflected direct radiation is:

$$E_{refl\_dir} = 0.5 f_{eff} f_{svv\_eq} I_{diff\_eq} \qquad (29)$$

As shown in Fig. 8, the equivalent sky view factor (f_{svv_eq}) is calculated according to equivalent angles in two directions (θ_{v_eq} and θ_{h_eq}). θ_{v_eq} and θ_{h_eq} can be calculated based on the deviation of the human body to the center line of the equivalent window (d_{e1} and d_{e2}), the equivalent window height (h_{refl}), the equivalent window width (equals to window width w), the window sill height (h_0), and the equivalent distance (d_e, $=0.5h_1$) between the human body and the equivalent window. Based on θ_{v_eq} and θ_{h_eq}, f_{svv_eq} can be calculated as follows:

$$d_{e2} \geq \frac{h_{refl}}{2}: \quad f_{svv\_eq} = [sin(tan^{-1}\frac{d_{e2}+\frac{h_{refl}}{2}}{d_e}) - sin(tan^{-1}\frac{d_{e2}-\frac{h_{refl}}{2}}{d_e})] \times \frac{\theta_{h\_eq}}{360} \qquad (30)$$

$$d_{e2} < \frac{h_{refl}}{2}: \quad f_{svv\_eq} = [sin(tan^{-1}\frac{\frac{h_{refl}}{2}+d_{e2}}{d_e}) + sin(tan^{-1}\frac{\frac{h_{refl}}{2}-d_{e2}}{d_e})] \times \frac{\theta_{h\_eq}}{360} \qquad (31)$$

$$h_{refl} = \frac{h}{tan(alt)} \cos cos\ \gamma \qquad (32)$$

$$d_{e1} = \left| d_0 - \frac{(h/2+h_0)}{tan(alt)} \sin sin\ \gamma \right| \qquad (33)$$

$$d_{e2} = \left| \frac{(h/2+h_0)}{tan(alt)} \cos cos\ \gamma - d \right| \qquad (34)$$

$$d_{e1} \geq \frac{w}{2}: \quad \theta_{h\_eq} = tan^{-1}\frac{d_{e1}+\frac{w}{2}}{d_e} - tan^{-1}\frac{d_{e1}-\frac{w}{2}}{d_e} \qquad (35)$$

$$d_{e1} < \frac{w}{2}: \quad \theta_{h\_eq} = tan^{-1}\frac{\frac{w}{2}+d_{e1}}{d_e} + tan^{-1}\frac{\frac{w}{2}-d_{e1}}{d_e} \qquad (36)$$

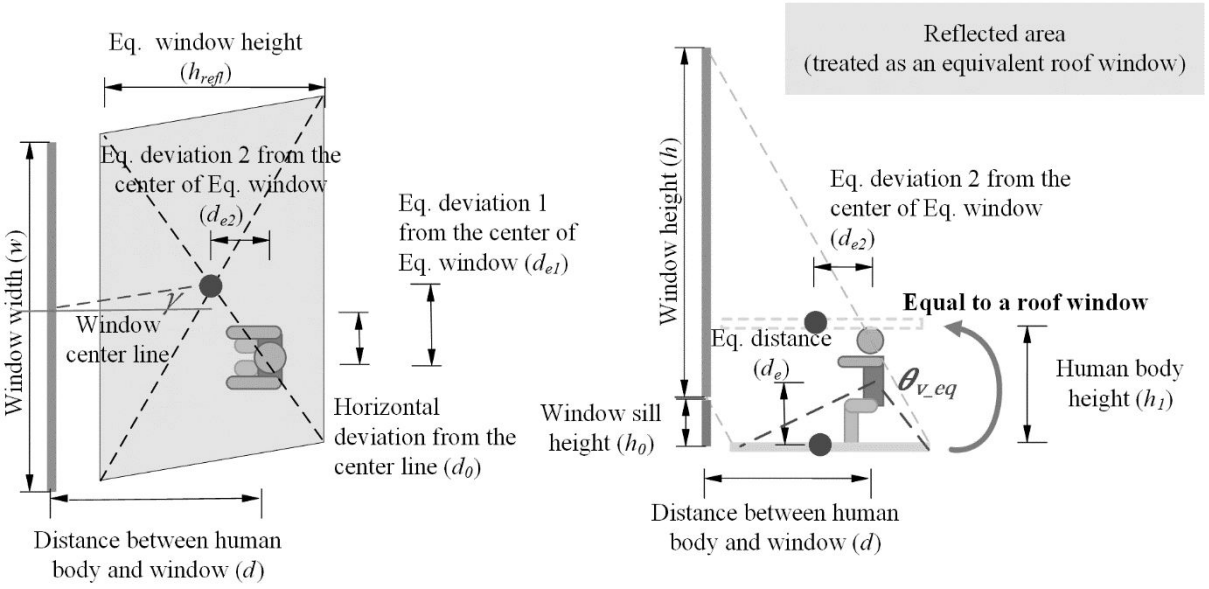

Fig. 8. Reflected direct solar radiation calculation: parameters for the equivalent window.

Calculation of E_{refl_diff}. For reflected diffuse radiation (E_{refl_diff}), the sky view factor of the body feet (f_{svv_feet}) is first calculated in a way similar to the revised diffuse radiation (see section 2.3.3.1). As shown in Fig. 9, f_{svv_feet} is based on angles in two directions: the horizontal angle (θ_h, same as that in Fig. 4(b)) and the vertical angle (θ_{v_feet}). θ_{v_feet} is decided by the vertical distance between the window center line and the feet (d_{feet}, $=h_0+0.5h$), the window sill height

https://doi.org/10.1016/j.buildenv.2020.107421
https://escholarship.org/uc/item/78f0b543

(h_0), and the distance between the human body and the window (d). f_{svv_feet} is calculated as below:

$$f_{svv\_feet} = [sin(tan^{-1}\frac{d_{feet}+\frac{h}{2}}{d}) - sin(tan^{-1}\frac{d_{feet}-\frac{h}{2}}{d})] \times \frac{\theta_h}{360} \quad (37)$$

Similar to Eq. (14), with the angle formed by the feet and the window sill ($\theta_{v\_sill\_feet}$), the actual outdoor diffuse radiation for indoor feet (I_{diff_feet}) is calculated as below:

$$I_{diff\_feet} = 0.8I_{diff} + (4.7 - 0.05\times alt) \times I_{diff} \times \frac{(90-|alt-0.5\theta_{v\_feet}-\theta_{v\_sill\_feet}|)\times(90-|\beta-\gamma|)}{90\times 90} \quad (38)$$

$$\theta_{v\_feet} = tan^{-1}\frac{d_4+\frac{h}{2}}{d} - tan^{-1}\frac{d_4-\frac{h}{2}}{d} \quad (39)$$

$$\theta_{v\_sill\_feet} = tan^{-1}\frac{h_0}{d} \quad (40)$$

And the final reflected diffuse radiation on the body is:

$$E_{refl\_diff} = 0.5f_{eff}f_{svv\_feet}T_{sol}I_{diff\_feet}R_{floor} \quad (41)$$

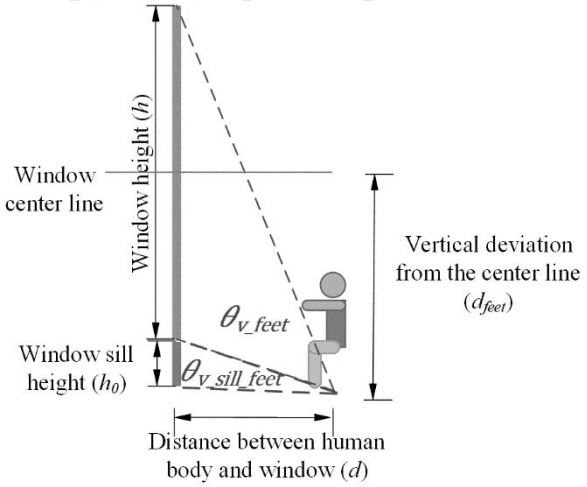

Fig. 9. Reflected diffuse solar radiation calculation: sky view factor of the human body feet.

The total reflected solar radiation flux is:

$$E_{refl} = E_{refl\_dir} + E_{refl\_diff} \quad (42)$$

2.3.4 Annual solar heat gain

By using global coordinates for window/occupant/sun angles, the HNU Solar Model is capable of performing annual simulations useful in energy simulation and environmental evaluation. In this way, it extends the applicability of SC Model, as does the DC Model [19]. Annual weather data can be obtained from a weather data website (https://www.ladybug.tools/epwmap/).

3 Results

3.1 Solar radiation at indoor points: comparisons of experimental results with those from DC method

Fig. 10 illustrates indoor and outdoor solar radiant fluxes between September 29th and October 1st. As shown in Fig. 10(a), the outdoor solar radiation (whether direct or diffuse) kept increasing since 7:00 and reached its peak at 12:00 (600-800 W/m^2 for direct normal radiation, and about 200 W/m^2 for diffuse radiation). In the afternoon, outdoor solar radiation kept decreasing from the peak value to 0 until 18:00. As shown in Fig. 10(b), for the four indoor points

(every two points at one position in Fig. 2(b)), since the chamber had a west window and direct solar radiation entered indoor space only in the afternoon, the indoor solar radiation in the morning was much weaker than that in the afternoon. In the morning (before 12:00), the indoor solar radiation was less than 50 W/m^2. In the afternoon, since position A was closer to the west window than position B, position A experienced the intense radiation (>200 W/m^2) since 13:00, which was one hour earlier than position B. The indoor solar radiation peaked at W/m^2 around 15:00, and then decreased to 0 at 18:00. The indoor solar radiation during the period from 9:00 to 17:00 was used to analyze the errors of the simulated indoor solar radiation by the DC method. Here, we use the coefficient of variation of the root mean square error, i.e., *CVRMSE,* which is the ratio of *RMSE* to the average actual value, as the error indicator. Through the comparison between the measured and the simulated indoor solar radiation, the *CVRMSE* values were 15.2%, 16.7%, 18.8%, and 23.3% for the vertical sensor at position A, the vertical sensor at position B, the horizontal sensor at position A, and the horizontal sensor at position B, respectively. The average values for the four points above were 150.6, 115.8, 90.3, and 64.1 W/m^2, respectively. The *CVRMSE* values indicate that the DC method is valid for predicting indoor solar radiation.

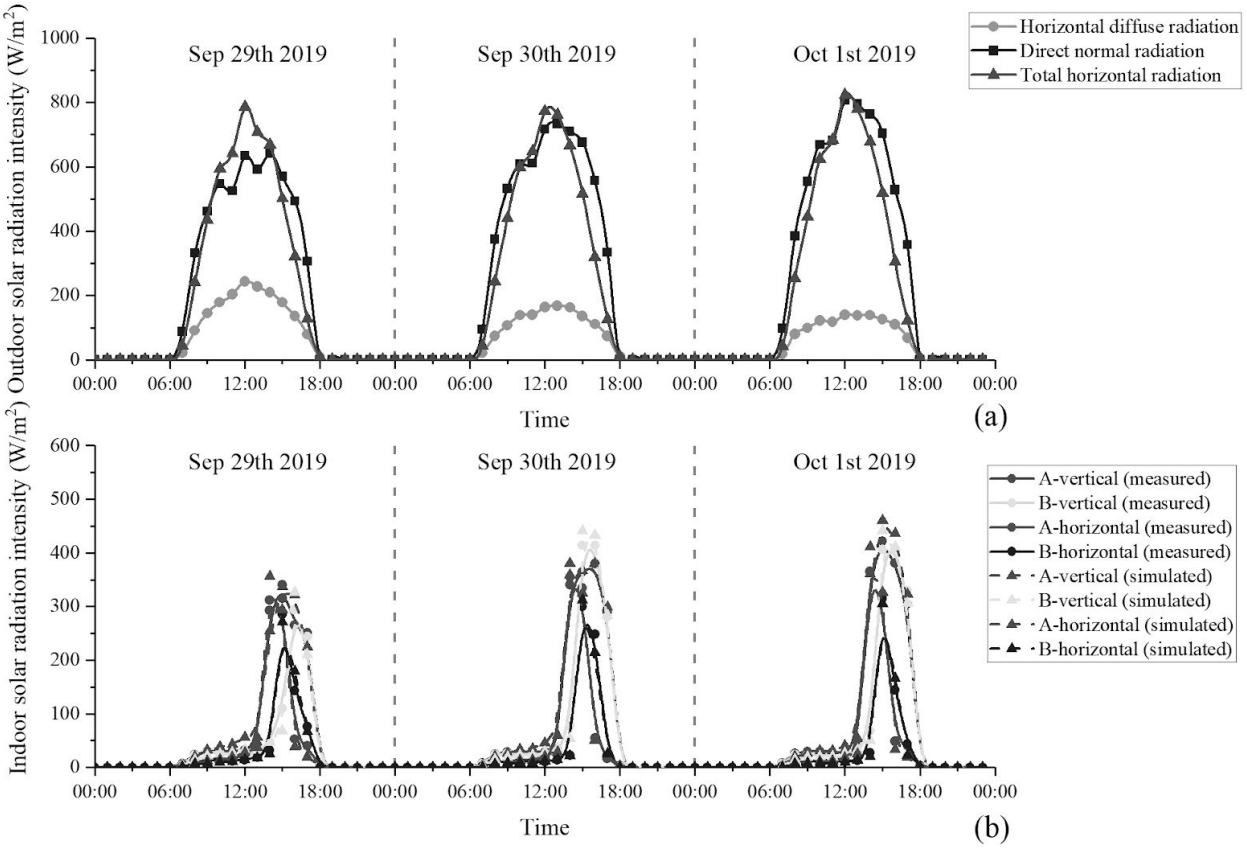

Fig. 10. Solar irradiation (W/m^2): (a) indoors and (b) outdoors.

3.2 Solar heat gain of human body indoors: comparisons of DC and HNU Solar Models

https://doi.org/10.1016/j.buildenv.2020.107421
https://escholarship.org/uc/item/78f0b543

In section 3.2, when calculating Delta MRT, the human body indoors was set at four positions, i.e., 0.5, 1.0, 1.5, and 2.0 m to the window, without horizontal deviations from the window center line.

3.2.1 Diffuse radiation

Fig. 11 illustrates the hourly Delta MRT by diffuse solar radiation with differently oriented windows. The peak diffuse radiation on the human body indoors with west, east, south, and north windows appears at around 15:00, 9:00, 12:00, and 12:00, respectively. When the human body is 1 m from the window, the Delta MRT by diffuse radiation can reach up to around 7°C with the west, east, and south windows, and to around 4°C with the north window. Besides, the differences of the Delta MRT by the HNU Solar and the DC Models are less than 1°C in most cases.

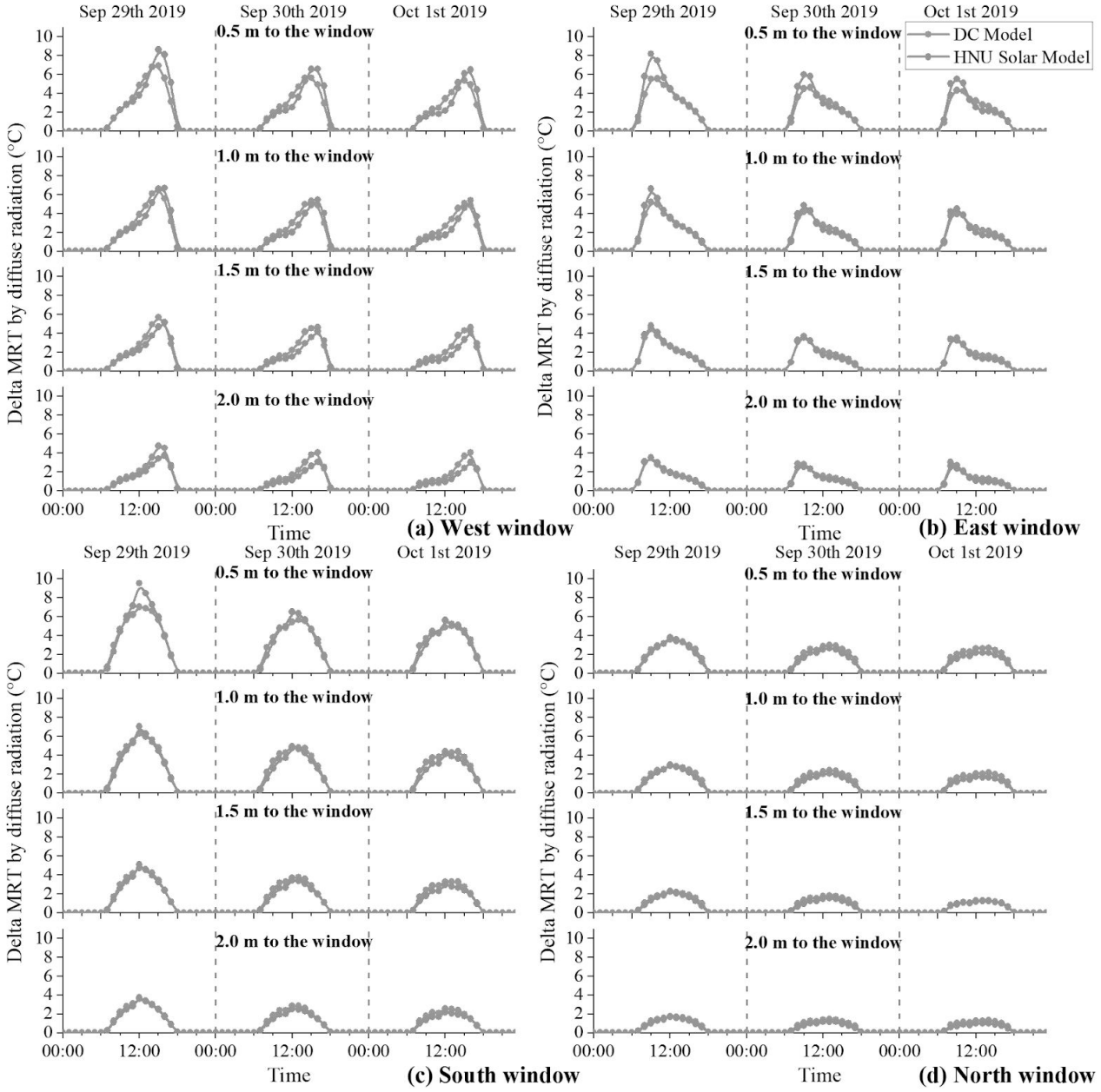

https://doi.org/10.1016/j.buildenv.2020.107421
https://escholarship.org/uc/item/78f0b543

Fig. 11. Delta MRT by diffuse solar radiation on the human body with (a) the west window, (b) the east window, (c) the south window, and (d) the north window

3.2.2 Direct radiation

Fig. 12 illustrates the hourly Delta MRT by direct solar radiation with different direction windows. The peaked direct radiation on the human body indoors with the west, east, and south windows appears at around 15:00, 9:00, and 12:00, respectively, and the peak Delta MRT can be up to about 20°C when the human body is 0.5 or 1.0 m to the window except for the north window. For west and east windows, the Delta MRT is zero in the morning and the afternoon, respectively. For a north window, the Delta MRT is always zero. The differences of Delta MRT values by the HNU Solar and the DC Models are usually less than 2°C. Since the Delta MRT by direct solar radiation can be 10-20°C, it is reasonable to say that the HNU Solar Model well predicts direct solar radiation on the human body indoors.

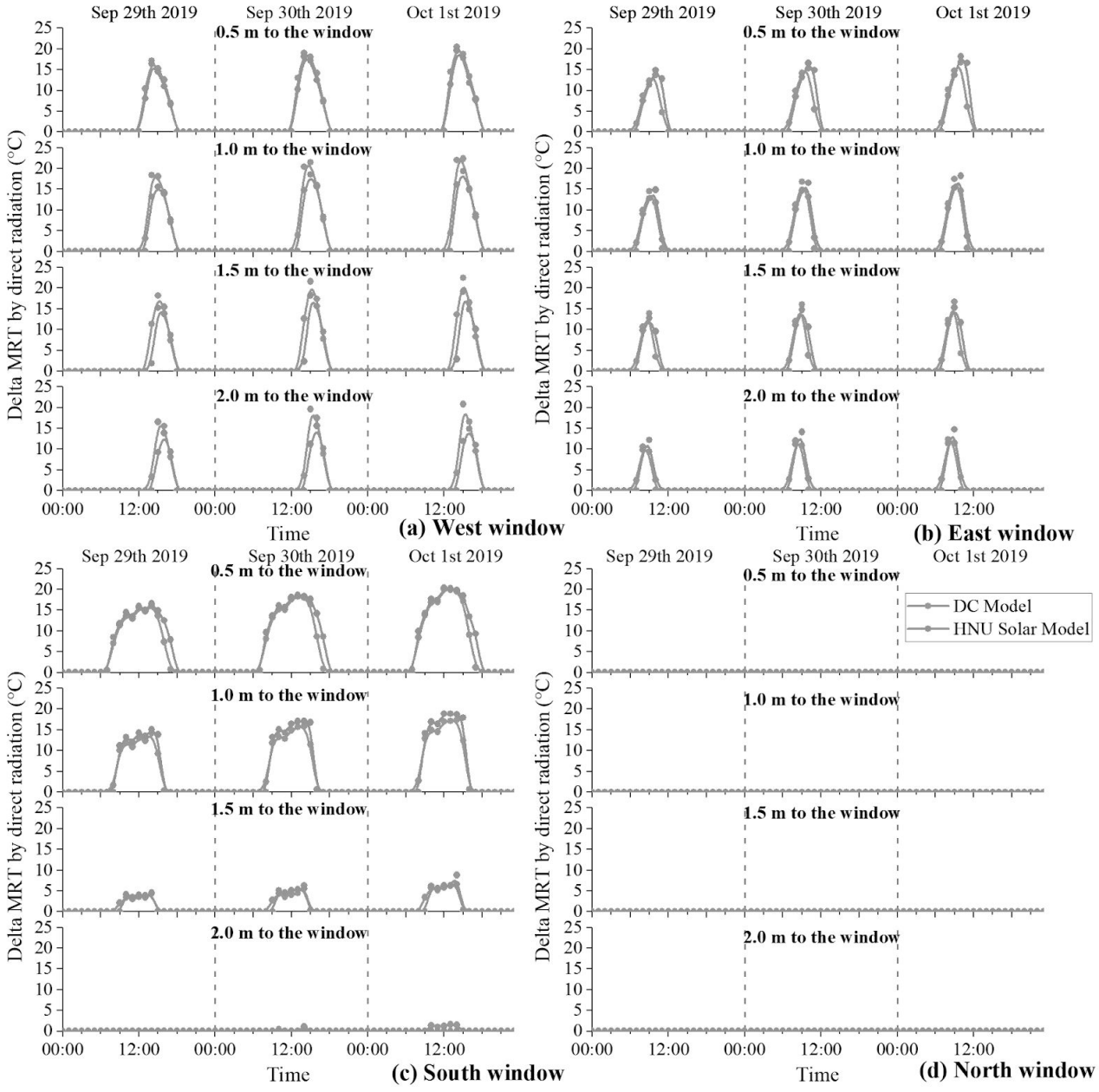

Fig. 12. Delta MRT by direct solar radiation on the human body with (a) the west window, (b) the east window, (c) the south window, and (d) the north window

3.2.3 Reflected radiation

Fig. 13 illustrates the hourly Delta MRT by reflected solar radiation with different direction windows. Corresponding to the Delta MRT by diffuse and direct radiation (Fig. 11 and 12), the peaked diffuse radiation on the human body indoors with the west, east, and south windows appears at around 15:00, 9:00, and 12:00, respectively. The peak Delta MRT values by reflected radiation are 2-4°C, except that with a north window (usually less than 0.2°C). The differences of Delta MRT values by the HNU Solar and the DC Models are less than 0.5°C in most cases.

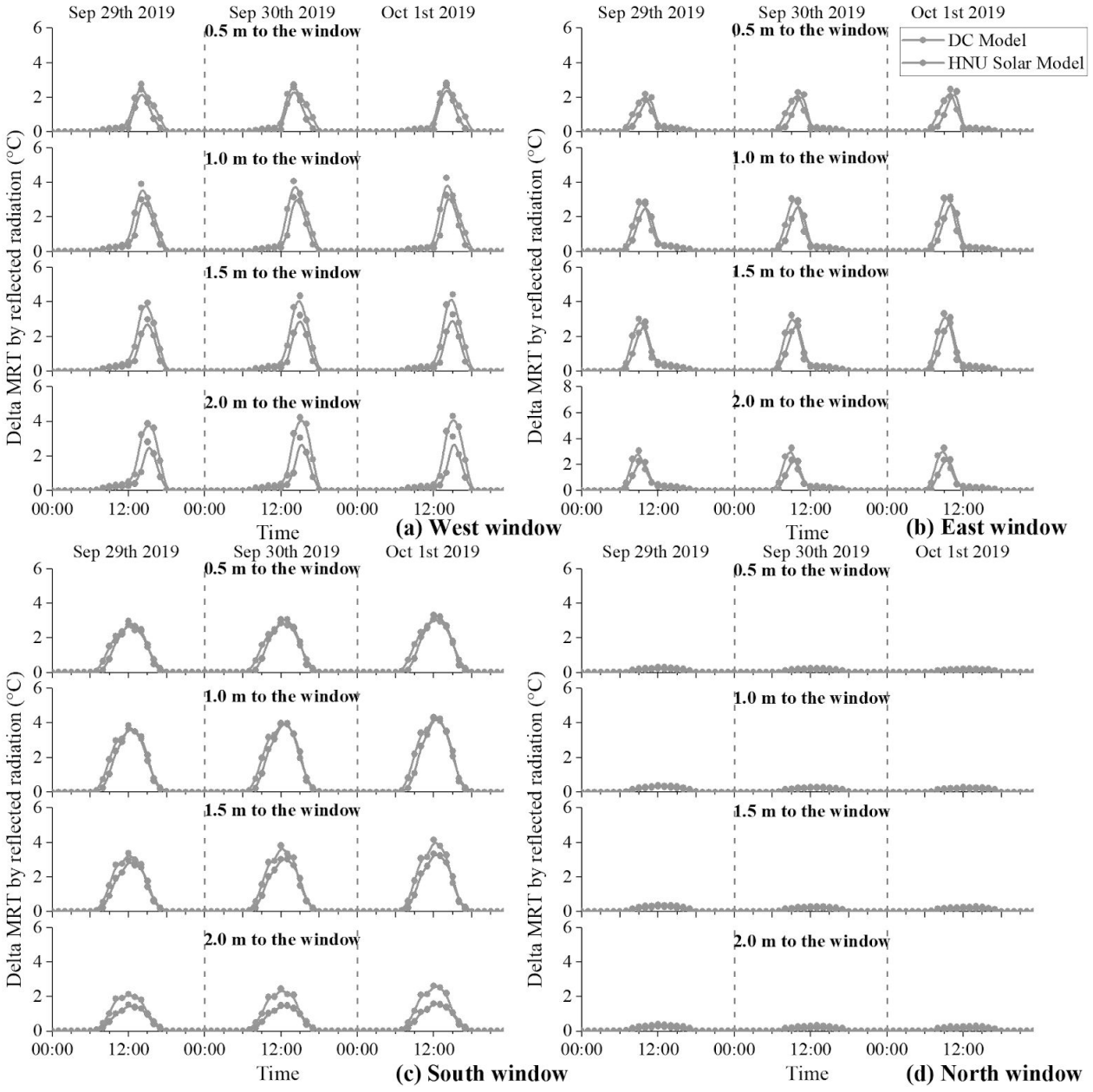

Fig. 13. Delta MRT by reflected solar radiation on the human body with (a) the west window, (b) the east window, (c) the south window, and (d) the north window

3.2.4 Total radiation

The Delta MRT by total solar radiation is the sum of those by diffuse, direct, and reflected solar radiation. Fig. 14 illustrates the hourly Delta MRT by total solar radiation with different windows. The peaked total radiation on the human body indoors with west, east, south, and north windows appears at around 15:00, 9:00, 12:00, and 12:00, respectively. And the peak Delta MRT can be about 30°C when the human body is 0.5 or 1.0 m away from the window. In most cases, the differences of Delta MRT values by the HNU Solar and DC Models are usually less than 2°C. Nonetheless, for the west or the east window, the differences sometimes can be higher than 5°C, mainly caused by the

difference of direct solar radiation on the human body (see Fig. 12). When calculating the direct solar radiation by the HNU Solar Model, the human body is simplified as a vertical stick at a certain point indoors, whereas the manikin of the DC model is closer to the real human body, which occupies three-dimension space indoors. The simplified body model in the HNU Solar Model would result in large deviations with the highly dynamic direct solar radiation (like that from the west window, which changes faster than that from the south window, see Fig. 12). To be specific, with highly dynamic direct solar radiation, there are more chances that the manikin of the DC Model still receives direct solar radiation (like on legs or part of the body trunk) when the vertical stick of the HNU Solar Model receives no direct solar radiation. From this perspective, the HNU Solar Model is more suitable for predicting solar radiation on occupants with south or north windows.

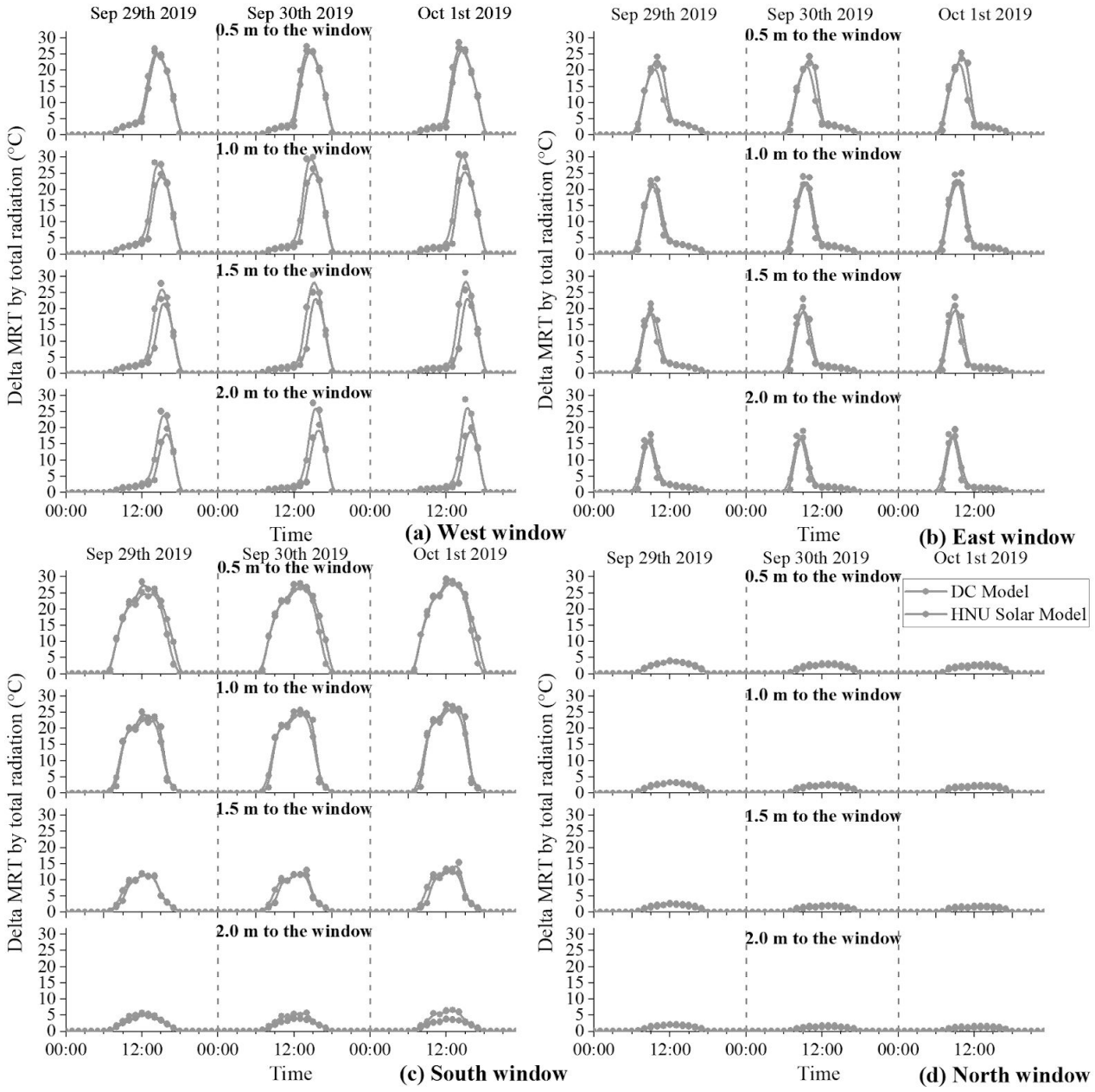

Fig. 14. Delta MRT by total solar radiation on the human body with (a) the west window, (b) the east window, (c) the south window, and (d) the north window

Further, we calculated the errors (*CVRMSE*) of the HNU Solar Model. We only used the data of Delta MRT values during the daytime 8:00-17:00. The errors were calculated under two circumstances, i.e., when the Delta MRT is higher than 0 and is higher than 4°C (we use Delta MRT≥3°C instead of MRT≥4°C for the north window condition where the maximum Delta MRT is lower than 4°C). The 4°C Delta MRT corresponds to a 2°C increase in operative temperatures (assuming the air temperature is unchanged), resulting in apparent changes in human thermal perceptions [39-41]. Table 1 shows the errors of the HNU Solar Model (the results by the DC Model are regarded as the true values). When the Delta MRT is higher than 0, the errors of the HNU Solar Model are usually less than 25% when the human body is less

than 2 m away from the window. When the Delta MRT is higher than 4°C, the errors of the HNU Solar Model are usually less than 20% when the human body is less than 2 m away from the window. The results in Table 1 indicate that the HNU Solar Model is much better for predicting the intense solar radiation on a human body (Delta MRT>4°C).

Table 1. Errors of the HNU Solar Model*.

	Distance to window			
Circumstance	0.5 m	1.0 m	1.5 m	2.0 m
When Delta MRT>0°C				
West window	11.8 (13.4%)	11.5 (29.2%)	10.0 (21.4%)	8.6 (32.3%)
South window	19.2 (15.4%)	16.0 (13.3%)	7.7 (19.9%)	3.8 (36.0%)
East window	8.4 (10.6%)	7.9 (23.2%)	6.4 (38.6%)	4.9 (31.1%)
North window	2.6 (15.3%)	2.2 (17.7%)	1.79 (19.9%)	1.4 (23.2%)
When Delta MRT≥4°C				
West window	18.1 (11.2%)	19.7 (23.3%)	19.2 (17.0%)	18.7 (25.2%)
South window	21.0 (9.0%)	17.5 (12.7%)	10.1 (17.9%)	5.4 (34.8%)
East window	16.0 (8.6%)	15.4 (18.0%)	16.5 (27.1%)	13.8 (19.0%)
North window (MRT≥3°C)	3.4 (8.2%)	3.15 (3.7%)	-	-

*: The results are expressed as *average (CVRMSE)*, and the average values were obtained by the DC Model.

3.3 Annual prediction performance

To evaluate the annual prediction performance of the HNU Solar Model, we used the DC and the HNU Solar Models to calculate the annual Delta MRT by solar radiation, respectively. The human body was set at the indoor position which is 1 m away from the window (no horizontal deviation from the window center line). 1 m from the window indoors is often affected by solar radiation in practice. Input variables of the room, manikin, and window were not changed. The analysis period was 8:00-17:00 during the daytime. Table 2 list the results by the DC and the HNU Solar Models. In the weather data file, sky cover is the fraction of the sky covered by cloud. The value of sky cover is 0-10 (tenths of coverage). For example, 1 means 10% of the sky is covered by cloud. The small sky cover value means that less direct solar radiation is blocked by the cloud. The results in Table 2 are divided into two groups: one with all-sky cover data, the other with the sky cover value less than 3 (less than 30% of the sky is covered). The average values were obtained by the DC Model. With all-sky cover values, when Delta MRT is higher than 4°C, the *CVRMSE* values of the HNU Solar Model are less than 30%, 2-6% lower than when Delta MRT is higher than 0. With sky cover values lower than 3, the *CVRMSE* values when Delta MRT is higher than 4°C can be further reduced by 2-6% compared to those with all-sky cover values. The results in Table 2 indicate that the HNU Solar Model is more proper for predicting strong solar radiation on a human body.

Table 2. Annual prediction performance of the HNU Solar Model.

	Delta MRT>0°C		Delta MRT≥4°C	
Condition	Average* (°C)	*CVRMSE*	Average* (°C)	*CVRMSE*
All-sky cover values				
West window	6.7	32.8%	9.7	27.2%
South window	8.0	26.5%	10.4	22.6%

East window	6.1	35.9%	9.3	29.5%
North window	3.7	14.7%	5.4	12.8%
Sky cover values<3				
West window	8.7	29.3%	12.9	25.1%
South window	12.7	18.3%	15.2	16.6%
East window	8.6	31.8%	14.0	25.6%
North window	3.4	13.0%	5.2	10.6%

*: The average values were obtained by the DC Model.

4 Discussion

4.1 Comparison among DC, SC, and HNU Solar Models

This section summarizes the differences among DC, SC, and HNU Solar Models in terms of input variables, applicable occasions, and calculation demands.

For input variables, as shown in Table 3, besides window transmittance and floor reflectance, the DC Model needs an entire room geometry (including the window) and a manikin model consists of 363 meshes. The SC Model needs 11 input variables but no geometry models. Some input variables of the SC Model, like f_{bes} and *SHARP*, need to be roughly estimated by the users, and the SC Model does not provide detailed ways to calculate them. Compared to the SC Model, the HNU Solar Model needs five more input variables. Some of the new variables (like horizontal deviation (d_0)) are related to new factors (like body position) affecting the solar radiation on a human body. Some variables (like window direction and front-body azimuth (azi_{body})) are used to calculate some key inputs (like *SHARP*), which are also used in the SC Model. Along with the model-establishment procedure of three models (see section 2.3), it can be seen that in terms of the calculation complexity, the HNU Solar Model is between the DC Model and the SC Model, and relatively simple to use compared to the DC Model.

Table 3. Input variables of the DC and SC Models.

Items	DC Model	SC Model	HNU Solar Model
Building	Room geometry Window geometry Window transmittance (T_{sol}) Floor reflectance (R_{floor})	Window height (h) Window width (w) Window transmittance (T_{sol}) Floor reflectance (R_{floor})	Window height (h) Window width (w) Window transmittance (T_{sol}) Floor reflectance (R_{floor}) Window sill height (h_0) Window direction
Human body	Short-wave absorptivity (α_{SW}) Manikin model Manikin position	Short-wave absorptivity (α_{SW}) Window-body distance (d) *SHARP* The body fraction exposed to solar beam radiation (f_{bes})	Short-wave absorptivity (α_{SW}) Window-body distance (d) Horizontal deviation (d_0) Front-body azimuth (azi_{body})
Climate data	Sun altitude (alt) Sun azimuth (azi) Direct normal radiation (I_{dir}) Diffuse radiation (I_{diff})	Sun altitude (alt) Direct normal radiation (I_{dir})	Sun altitude (alt) Sun azimuth (azi) Direct normal radiation (I_{dir}) Diffuse radiation (I_{diff})

As stated in Zani's study [36], the DC Model can be used to calculate the body solar heat gain with complex

window shapes, indoor layouts, and outdoor surroundings. The SC Model is more suitable for estimating the Delta MRT within a specific representative design condition. While the HNU Solar Model is between these two models: HNU Solar Model is able to do annual calculations with various body positions indoors, but cannot handle complex window geometries and indoor layouts.

For calculation demand, the DC Model needs *Rhinoceros* + *Grasshopper* to build a room model and a manikin and needs *Radiance* to run solar radiation simulations. While both the SC and the HNU Solar Models only need computer programming language (like Python) for calculation. Thus the SC and the HNU Solar Models are much easier to be used and friendlier for people who are not familiar with *Rhinoceros* and *Radiance*. Also, due to the simplified calculate procedure, the SC and the HNU Solar Models are much faster than the DC Model when calculating the Delta MRT. For calculating the annual Delta MRT at one specific position indoors, the DC Model needs about 7 minutes, while the original and the HNU Solar Models need about 5 seconds (tested by a laptop owned by the authors, Intel Core i7-9750H, CPU 2.60GHz, Windows 10, 64-bit, 8G RAM).

4.2 Potential applications of this study

The HNU Solar Model proposed in this study may contribute to (1) space-scale indoor environment evaluations, and (2) annual energy prediction of building HVAC systems. Two examples are shown in Fig. 15:

(1) For space-scale indoor environment evaluations, since the HNU Solar Model includes the effects of the human body position indoors, in a certain room with a window, Delta MRT in different positions indoors can be easily calculated. Fig. 15(a) shows the mapping of Delta MRT by solar radiation in a room with a south window at 10:00 and 15:00 on September 29th. The input variables are the same as those for results in section 3.2.4 except that Delta MRT values at multiple positions indoors were calculated. It is clear that the indoor area close to the window (the distance is less than 1 m) is significantly affected by the solar radiation, and the Delta MRT can be higher than 10°C at 10:00 and 15:00. The north-east corner and the north-west corner of the room are almost not affected by the solar radiation at 10:00 and 15:00, respectively. Besides, the occupant should be at least 2 m away from the window to avoid significant solar radiation (Delta MRT>4°C).

(2) The HNU Solar Model makes it possible to calculate annual HVAC set-point corrections. Here, we use the operative temperature correction which is half of Delta MRT [35], as the HVAC set-point corrections. For example, when the positive operative temperature correction is 2°C, if there are no other supplementary cooling for occupants, the set-point should be correspondingly lowered by 2°C for occupants' thermal comfort. In summer, this correction means that more energy is needed for cooling; while in winter, it means less energy is needed for heating. Fig. 15(b) illustrates a case of set-point corrections calculated by the HNU Solar Model. In this case, the room has a south window

(1.5 m in width, 2.0 m in height, with 0.5 transmittance and 1.0 m window sill). When the human body is 1.5 m away from the window, high operative temperature corrections (>5°C) mainly appear during the winter daytime, which means that occupants feel warmer due to the solar radiation. Thus it is possible to set lower indoor air temperature of the HVAC system and save much heating energy in winter. Nonetheless, if the occupant is close to the window like 0.5 m away, although the heating energy can be saved in winter, the set-point correction can be higher (like higher than 5°C) than the available changes of HVAC set-points for compensating the solar heat on the human body in summer. From the perspective of energy savings, to reduce the considerable overheating of solar radiation in summer, the best solution is to use window shades, tinted window glass with low transmittance, or adjust the window geometry size. The effects of latter two approaches can be estimated by using the HNU Solar Model.

Furthermore, it should be noted that the set-point correction indicates how environmental factors should be adjusted to maintain the thermal comfort of occupants exposed to solar radiation, from the perspective of the heat balance of occupants. It does not involve the trade-off of individual thermal comfort among occupants at different locations in the same shared space, which is another complicated topic on individual differences in practice [42, 43] and beyond the content of the model. Lowering set-points for compensating solar heat on the occupant in summer might cause overcooling for other occupants far away from the window, and it needs much additional energy. A possible solution is to use local cooling systems for compensating solar heat on occupants. Local cooling systems include personal ventilation [44, 45], fans [46-48], local radiant cooling [40, 49], and so on. They need very less additional energy and will not overcool other occupants away from the window. Nonetheless, the effects of local cooling on occupants exposed to solar radiation are beyond the topic of this study, and thus they are not analyzed in detail.

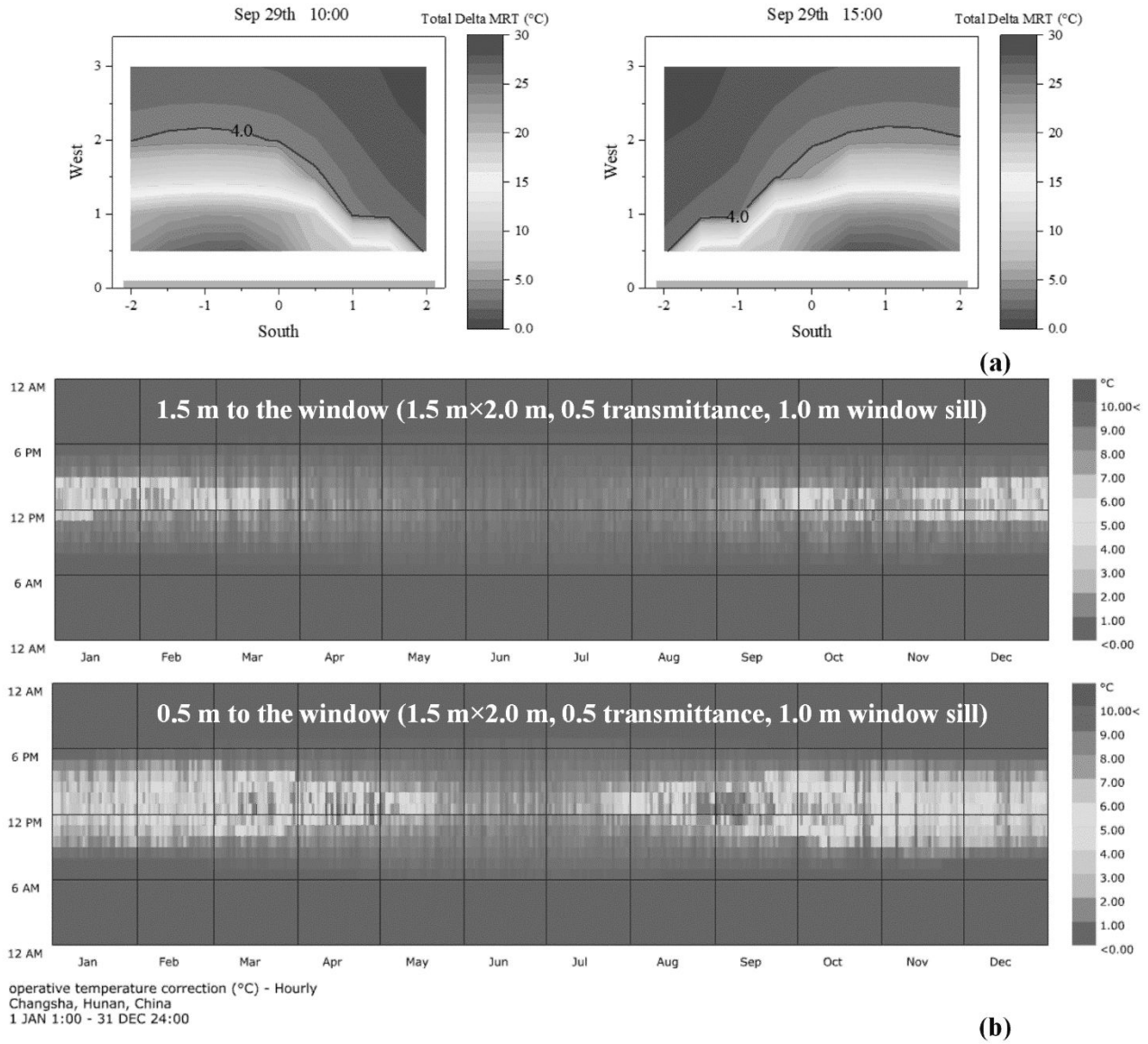

Fig. 15. Potential application of this study: (a) the space-mapping of Delta MRT values by solar radiation, and (b) the annual operative temperature corrections of HVAC systems.

4.3 Limitations

(1) In the HNU Solar Model, the diffuse radiant intensity at one point in the sky is used to represent the average flux passing through the window aperture and irradiating the human body. For a large window or a person close to the window, this calculation maybe overestimate the diffuse radiation impact on the human body. The glass transmittance is also independent of solar incidence angle which will overestimate many daily and annual solar transmission calculations.

(2) When calculating the direct solar radiation, the human body is simplified as a vertical stick, whereas an actual seated body is much more complicated.

(3) The experimental results of solar radiation were obtained on sunny days, and thus the HNU Solar Model does

not include the effect of cloudy weather conditions.

(4) The HNU Solar Model is still a simplified method to calculate the solar heat gain of an indoor human body. It may have errors when the building has complicated outdoor surroundings or indoor furniture that blocks solar radiation onto the occupant.

5 Conclusions

This paper proposes the HNU Solar Model and demonstrates its use in calculating the solar heat gain (Delta MRT) of the human body indoors. The results were compared with those calculated by the DC Model. The main conclusions are summarized below:

(1) For diffuse solar radiation on a human body indoors, the HNU Solar Model calculates the sky view factor by a sky-annulus-fraction method and estimates the window-transmitted radiant flux using a simplified linear estimation of average sky radiation intensity. The Delta MRT difference between the HNU Solar and the DC Models is less than 1°C in most cases.

(2) For direct solar radiation on a human body indoors, we defined the virtual body shadow for calculating the fraction of the human body exposed to the solar beam with dynamic sun positions. And the difference of Delta MRT values by direct solar radiation between the HNU Solar and the DC Models is usually less than 2°C.

(3) For reflected solar radiation on a human body indoors, we proposed the concept of the equivalent window to calculate the reflected direct radiation, and we also calculate the reflected diffuse radiation based on the point near the human feet. The difference of Delta MRT values by reflected solar radiation between the HNU Solar and the DC Models is usually less than 0.5°C.

(4) The HNU Solar Model has higher accuracy when the human body is under stronger solar radiation. When the Delta MRT is higher than 0, the *CVRMSE* of the HNU Solar Model is usually less than 25% when the human body is less than 2 m away from the window. When the Delta MRT is higher than 4°C, the *CVRMSE* of the HNU Solar Model is usually less than 20% when the human body is less than 2 m away from the window. When the human body is close to the window, as compared with the DC Model, the HNU Solar Model overestimates the Delta MRT.

(5) Compared with the DC Model, the HNU Solar Model is much easier to use since it does not need a complicated building model or manikin model. The HNU Solar Model also has advantages in calculation speed. For a specific position of the human body indoors, the HNU Solar Model only needs five seconds to its annual Delta MRT by solar radiation, while the DC Model needs about seven minutes.

Acknowledgments

This study was sponsored by the National Natural Science Foundation of China (Project No. 51878255). The

authors would also like to express heartfelt thanks to Andrea Zani who provided the DC Model file for our research work.

References

[1] K. Connelly, Y. Wu, J. Chen, Y. Lei, Design and development of a reflective membrane for a novel Building Integrated Concentrating Photovoltaic (BICPV)'Smart Window'system, Applied energy, 182 (2016) 331-339.
[2] M. Tripathy, P. Sadhu, S. Panda, A critical review on building integrated photovoltaic products and their applications, Renewable and Sustainable Energy Reviews, 61 (2016) 451-465.
[3] J. Peng, D.C. Curcija, A. Thanachareonkit, E.S. Lee, H. Goudey, S.E. Selkowitz, Study on the overall energy performance of a novel c-Si based semitransparent solar photovoltaic window, Applied Energy, 242 (2019) 854-872.
[4] C. Qiu, Y.K. Yi, M. Wang, H. Yang, Coupling an artificial neuron network daylighting model and building energy simulation for vacuum photovoltaic glazing, Applied Energy, 263 (2020) 114624.
[5] S.-Y. Wu, L. Xu, L. Xiao, Performance study of a novel multi-functional Trombe wall with air purification, photovoltaic, heating and ventilation, Energy Conversion and Management, 203 (2020) 112229.
[6] H. Li, H. Yang, Potential application of solar thermal systems for hot water production in Hong Kong, Applied Energy, 86 (2) (2009) 175-180.
[7] A. Dahash, F. Ochs, M.B. Janetti, W. Streicher, Advances in seasonal thermal energy storage for solar district heating applications: A critical review on large-scale hot-water tank and pit thermal energy storage systems, Applied Energy, 239 (2019) 296-315.
[8] J. Prakash, D. Roan, W. Tauqir, H. Nazir, M. Ali, A. Kannan, Off-grid solar thermal water heating system using phase-change materials: design, integration and real environment investigation, Applied energy, 240 (2019) 73-83.
[9] S.K. Shah, L. Aye, B. Rismanchi, Multi-objective optimisation of a seasonal solar thermal energy storage system for space heating in cold climate, Applied Energy, 268 (2020) 115047.
[10] A. Yongga, N. Li, J. Long, Y. He, Thermal performance of a novel solar thermal facade system in a hot-summer and cold-winter zone, Solar Energy, 204 (2020) 106-114.
[11] K. Wang, N. Li, J. Peng, Y. He, Study on the optimizing operation of exhaust air heat recovery and solar energy combined thermal compensation system for ground-coupled heat pump, International Journal of Photoenergy, 2017 (2017).
[12] B. Yu, J. Hou, W. He, S. Liu, Z. Hu, J. Ji, H. Chen, G. Xu, Study on a high-performance photocatalytic-Trombe wall system for space heating and air purification, Applied energy, 226 (2018) 365-380.
[13] B. Yu, Q. Jiang, W. He, S. Liu, F. Zhou, J. Ji, G. Xu, H. Chen, Performance study on a novel hybrid solar gradient utilization system for combined photocatalytic oxidation technology and photovoltaic/thermal technology, Applied Energy, 215 (2018) 699-716.
[14] M. De Carli, M. Tonon, Effect of modelling solar radiation on the cooling performance of radiant floors, Solar energy, 85 (5) (2011) 689-712.
[15] K. Zhao, X.-H. Liu, Y. Jiang, Dynamic performance of water-based radiant floors during start-up and high-intensity solar radiation, Solar Energy, 101 (2014) 232-244.
[16] C. Xu, S. Li, X. Zhang, Application of the CPMV index to evaluating indoor thermal comfort in winter: Case study on an office building in Beijing, Build. Environ., 162 (2019) 106295.
[17] G. Liu, Z. Wang, C. Li, S. Hu, X. Chen, P. Liang, Heat exchange character and thermal comfort of young people in the building with solar radiation in winter, Build. Environ., (2020) 106937.
[18] R. Yang, H. Zhang, S. You, W. Zheng, X. Zheng, T. Ye, Study on the thermal comfort index of solar radiation conditions in winter, Build. Environ., 167 (2020) 106456.
[19] Z.J. Zhai, Critical Review and Quantitative Evaluation of Indoor Thermal Comfort Indices and Models Incorporating Solar Radiation Effects, Energy Build., (2020) 110204.
[20] S. Zhang, J. Fine, M.F. Touchie, W. O'Brien, A simulation framework for predicting occupant thermal sensation in perimeter zones of buildings considering direct solar radiation and ankle draft, Build. Environ., (2020) 107096.
[21] J. Wu, X. Li, J. Tu, L. Yang, Y. Yan, A PMV-based HVAC control strategy for office rooms subjected to solar radiation, Build. Environ., (2020) 106863.
[22] L.L. Fernandes, E.S. Lee, A. McNeil, J.C. Jonsson, T. Nouidui, X. Pang, S. Hoffmann, Angular selective window systems: Assessment of technical potential for energy savings, Energy Build., 90 (2015) 188-206.
[23] R. Zmeureanu, S. Iliescu, D. Dauce, Y. Jacob, Radiation from cold or warm windows: computer model development and experimental validation, Build. Environ., 38 (3) (2003) 427-434.
[24] H. Guo, M. Ferrara, J. Coleman, M. Loyola, F. Meggers, Simulation and measurement of air temperatures and mean radiant temperatures in a radiantly heated indoor space, Energy, 193 (2020) 116369.

[25] T. Kim, S. Kato, S. Murakami, J.-w. Rho, Study on indoor thermal environment of office space controlled by cooling panel system using field measurement and the numerical simulation, Build. Environ., 40 (3) (2005) 301-310.
[26] C. Marino, A. Nucara, M. Pietrafesa, Mapping of the indoor comfort conditions considering the effect of solar radiation, Solar Energy, 113 (2015) 63-77.
[27] C. Marino, P. Misiani, A. Nucara, M. Pietrafesa, The effect of the climatic condition on the radiant asymmetry, Int. J. Heat Technol., 35 (2017) S419-S426.
[28] M. La Gennusa, A. Nucara, G. Rizzo, G. Scaccianoce, The calculation of the mean radiant temperature of a subject exposed to the solar radiation—a generalised algorithm, Build. Environ., 40 (3) (2005) 367-375.
[29] M. La Gennusa, A. Nucara, M. Pietrafesa, G. Rizzo, A model for managing and evaluating solar radiation for indoor thermal comfort, Solar Energy, 81 (5) (2007) 594-606.
[30] A. Tzempelikos, M. Bessoudo, A. Athienitis, R. Zmeureanu, Indoor thermal environmental conditions near glazed facades with shading devices–Part II: Thermal comfort simulation and impact of glazing and shading properties, Build. Environ., 45 (11) (2010) 2517-2525.
[31] R.-L. Hwang, S.-Y. Shu, Building envelope regulations on thermal comfort in glass facade buildings and energy-saving potential for PMV-based comfort control, Build. Environ., 46 (4) (2011) 824-834.
[32] H. Zhang, R. Yang, S. You, W. Zheng, X. Zheng, T. Ye, The CPMV index for evaluating indoor thermal comfort in buildings with solar radiation, Build. Environ., 134 (2018) 1-9.
[33] E. Arens, T. Hoyt, X. Zhou, L. Huang, H. Zhang, S. Schiavon, Modeling the comfort effects of short-wave solar radiation indoors, Build. Environ., 88 (2015) 3-9.
[34] H. Tyler, S. Stefano, T. Federico, C. Toby, S. Kyle, P. Alberto, M. Dustin, CBE Thermal Comfort Tool, in, Center for the Built Environment, University of California Berkeley 2019.
[35] ANSI/ASHRAE, Standard 55-2017: Thermal environmental conditions for human occupancy, American Society of Heating, Refrigerating and Air-Conditioning Engineering, Atlanta, GA, (2017).
[36] A. Zani, A.G. Mainini, J.D. Blanco Cadena, S. Schiavon, E. Arens, A new modeling approach for the assessment of the effect of solar radiation on indoor thermal comfort, in: 2018 Building Performance Analysis Conference and SimBuild, 2018, pp. 181-188.
[37] M. Saxena, G. Ward, T. Perry, L. Heschong, R. Higa, Dynamic Radiance–Predicting annual daylighting with variable fenestration optics using BSDFs, Proceedings of SimBuild, 4 (1) (2010) 402-409.
[38] M.D. Steven, M. Unsworth, Standard distributions of clear sky radiance, Quarterly Journal of the Royal Meteorological Society, 103 (437) (1977) 457-465.
[39] Y. He, N. Li, W. Zhang, L. Zhou, Thermal comfort of sellers with a kind of traditional personal heating device (Huotong) in marketplace in winter, Build. Environ., 106 (2016) 219-228.
[40] Y. He, N. Li, X. Wang, M. He, D. He, Comfort, Energy Efficiency and Adoption of Personal Cooling Systems in Warm Environments: A Field Experimental Study, International journal of environmental research and public health, 14 (11) (2017) 1408.
[41] Y. He, X. Wang, N. Li, M. He, D. He, Heating chair assisted by leg-warmer: A potential way to achieve better thermal comfort and greater energy conservation in winter, Energy Build., 158 (2018) 1106-1116.
[42] Y. He, N. Li, N. Li, J. Li, J. Yan, C. Tan, Control behaviors and thermal comfort in a shared room with desk fans and adjustable thermostat, Build. Environ., 136 (2018) 213-226.
[43] Z. Wang, H. Zhang, Y. He, M. Luo, Z. Li, T. Hong, B. Lin, Revisiting individual and group differences in thermal comfort based on ASHRAE database, Energy Build., (2020) 110017.
[44] M. Dalewski, A.K. Melikov, M. Vesely, Performance of ductless personalized ventilation in conjunction with displacement ventilation: Physical environment and human response, Build. Environ., 81 (2014) 354-364.
[45] A. Lipczynska, J. Kaczmarczyk, A.K. Melikov, Thermal environment and air quality in office with personalized ventilation combined with chilled ceiling, Build. Environ., 92 (2015) 603-614.
[46] Y. He, W. Chen, Z. Wang, H. Zhang, Review of fan-use rates in field studies and their effects on thermal comfort, energy conservation, and human productivity, Energy Build., 194 (2019) 140-162.
[47] P. Raftery, J. Fizer, W. Chen, Y. He, H. Zhang, E. Arens, S. Schiavon, G. Paliaga, Ceiling fans: Predicting indoor air speeds based on full scale laboratory measurements, Build. Environ., 155 (2019) 210-223.
[48] Y. He, N. Li, H. Zhang, Y. Han, J. Lu, L. Zhou, Air-conditioning use behaviors when elevated air movement is available, Energy Build., (2020) 110370.
[49] Y. He, N. Li, M. He, D. He, Using radiant cooling desk for maintaining comfort in hot environment, Energy Build., 145 (2017) 144-154.